Technical Report

TR-06-01

Grain boundary corrosion of copper canister weld material

Rolf Gubner, Urban Andersson, Mats Linder,
Andrej Nazarov, Claes Taxén
Korrosionsinstitutet

January 2006

Svensk Kärnbränslehantering AB
Swedish Nuclear Fuel
and Waste Management Co
Box 5864
SE-102 40 Stockholm Sweden
Tel 08-459 84 00
+46 8 459 84 00
Fax 08-661 57 19
+46 8 661 57 19

Grain boundary corrosion of copper canister weld material

Rolf Gubner, Urban Andersson, Mats Linder,
Andrej Nazarov, Claes Taxén
Korrosionsinstitutet

January 2006

Executive summary

The proposed design for a final repository for spent fuel and other long-lived residues in Sweden is based on the multi-barrier principle. The waste will be encapsulated in sealed cylindrical canisters, which will then be placed in granite bedrock and surrounded by compacted bentonite clay. The canister design is based on a thick cast inner container fitted inside a corrosion-resistant copper canister.

During fabrication of the outer copper canisters there will be some unavoidable grain growth in the welded areas. As grains grow, they will tend to concentrate impurities within the copper at the new grain boundaries. The work described in this report was undertaken to determine whether there is any possibility of enhanced corrosion at grain boundaries within the copper canister, based on the recommendations of the report TR-01-09. Grain boundary corrosion of copper is not expected to be a problem for the copper canisters in a repository. However, as one step in the experimental verification it is necessary to study grain boundary corrosion of copper in an environment where it may occur. A literature study aimed to find one or several solutions that are aggressive with respect to grain boundary corrosion of copper. Copper specimens cut from welds of real copper canisters where exposed to aerated ammonium hydroxide solution for a period of 14 days at 80 degrees Celsius and 10 bar pressure. The samples were investigated prior to exposure using the scanning Kelvin probe technique to characterize anodic and cathodic areas on the samples. The degree of corrosion was determined by optical microscopy.

No grain boundary corrosion could be observed in the autoclave experiments, however, a higher rate of corrosion was observed for the weld material compared to the base material.

The work suggests that grain boundary corrosion of copper weld material is most unlikely to adversely affect SKB’s copper canisters under the conditions in the repository.

Contents

1 Introduction

The proposed design for a final repository for spent fuel and other long-lived residues in Sweden is based on the multi-barrier principle. The waste will be encapsulated in sealed cylindrical canisters, which will then be placed in granite bedrock and surrounded by compacted bentonite clay. The canister design is based on a thick cast inner container fitted inside a corrosion-resistant copper canister.

Copper lids and bottoms are made by forging of continuous-cast bars. The forged blanks are machined to the desired dimensions. It is noted in the report TR-02-07 that the grain size obtained in lids and bottoms is much coarser than in fabricated copper tubes. Welding of bottoms on copper tubes has been done with electron beam welding (EBW). Therefore, the samples of welds used in this study have been produced by the same technique.

During fabrication of the outer copper canisters there will be some unavoidable grain growth in the welded areas. As grains grow intermetallic phases are precipitated at the grain boundaries. The concern raised by Boyer /6/ was whether this concentration of impurities in the grain boundaries would be sufficient to provide for the possibility of grain boundary corrosion.

Very little information on grain boundary corrosion of pure copper is found in the literature. On the other hand, grain boundary corrosion on copper alloys e.g. 70:30 brass is relatively well established. On pure copper the dissimilarities in corrosion behaviour between different grain orientations seem to dominate over dissimilarities between grain surface and grain boundary.

1.1 Previous tests

Fennell and coworkers at AEA Technology have studied grain boundary effects during corrosion of copper on behalf of the SKB /1/. They used ‘bentonite-equilibrated Äspö groundwater’ containing 10 mM sodium carbonate and 20 ppm or 20,000 ppm sodium chloride, adjusted with NaOH to pH 10. A 28 days exposure at room temperature did not result in measurable grain boundary corrosion.

1.2 Observations of grain boundary corrosion on copper alloys

Leidheiser /2/ quotes 70:30 brass in ammonium hydroxide as an example of grain boundary corrosion. One of two parallel specimen was pretreated so that the grain boundaries were coated with varnish. For the other specimen, grain fields but not the boundaries were coated with varnish.

The two types of specimens where connected to each other and exposed to 1% NH_4OH solution. A galvanic current in the order of 3.3 mA/cm^2 was measured. The specimen with exposed grain boundaries behaved as anode.

1.3 Microelectrode study of grain related corrosion phenomena on copper.

Miyamoto and coworkers /3, 4/ studied the corrosion of high purity copper bicrystals. Using a scanning vibrating electrode technique they could detect local aberrations at the grain boundaries. Depending on the orientation of the exposed crystal planes, the grain boundary could behave as an anode or as a cathode. The site of the grain boundary developed into a grove or a ridge respectively. The authors conclude that corrosion anisotropy as well as grain boundary energy plays an important role in the formation of local cells at the grain boundary.

1.4 Theoretical aspects on the selection of solution intended to be aggressive with respect to grain boundary corrosion of copper

Local corrosion attacks at the site of a grain boundary may be caused by several different effect:

- the grain boundary corrodes because it is less noble than the grain surface, either because of an enrichment or depletion of alloying elements and impurities or because of a difference in surface energies.
- the grain boundary corrodes because it is very close to local cathodic regions in the vicinity of the grain boundary
- the grain boundary corrodes because the anodic dissolution of alloying elements and impurities, enriched at the grain boundary, results in a film of corrosion products that is less protective than the film formed at the grain surfaces.

The selection of solution intended to be aggressive with respect to grain boundary corrosion of copper is of course related to the nature of the cause of the local corrosion attack.

In the first case, a relatively high conductivity would seem to promote grain boundary corrosion since the whole grain surface can act as cathode.

In the second case, a relatively low conductivity would seem to promote local corrosion attack since the effects of local cathodic sites then is restricted to short distances. In solutions of higher conductivity, the effects of local cathodic sites would be ‘smeared out’ over the whole grain surfaces.

In the third case, it is not the metallurgical properties that are important, but the protective properties of the film of corrosion products. Clearly, if such a phenomenon exists, this would not be detected in a test where no corrosion film is formed. Conversely, the formation of an extensive film of corrosion products, in an experiment, might prevent grain boundary corrosion according to cases one and two from being observed.

Since grain boundary corrosion is not observed on pure copper one cannot say which of the three suggested causes that may be operative. A test solution composed to stimulate one effect may automatically counteract another. The preferred test matrix would contain one low conductivity solution and one high conductivity solution. Both used under conditions where there is no extensive film formation. In addition the matrix should contain one solution that promotes film formation.

Film formation is counteracted by low pH and low chloride concentrations. Film formation is promoted by high pH and/or high/moderately high chloride concentrations.

1.5 Suggested test matrix

It would be an advantage to show that the tests performed can detect grain boundary corrosion in systems where this occurs. The system quoted by Leidheiser above might be used.

Room temperature studies on pure copper (SKB copper) at high pH have already been performed at AEA Technology /1/. Ammonia and nitrite are known to be aggressive to copper alloys, primarily promoting stress corrosion cracking. In a search for worst possible solution with respect to grain boundary corrosion these compounds might well be included in all solutions since their effect is not likely to counteract grain boundary corrosion.

Air saturation of the solutions is likely to ensure sufficiently oxidising conditions.

A solution containing 1% NH_4OH was used in the first experiment. This solution is known to cause grain boundary corrosion of 70:30 brass.

An acidified (pH 4.0) 1 M NaCl plus 0.25 M triodium citrate plus 0.015 M CuCl solution was used in experiment 2. This solution was used by Mazza and Tochio /5/ for a study investigating factors influencing the susceptibility to intergrannular attack, stress corrosion cracking and dealloying attack of aluminum brass. However, it should be noted that the conditions created by this solution are far from real conditions present in the repository. This solution was used to demonstrate whether grain boundary corrosion can be induced on copper canister material.

2 Experimental programme

2.1 Sample preparation

The samples where provided by SKB. Electron beam welded samples where cylinders drilled out from welds (4 cm diameter) and labeled L006, L013, L015, L017, L019. (Table 2-1) All electron bream welded samples, except L013 where cut as indicated in Figure 2-1. Sample L013 was cut in parallel to the surface resulting in round samples.

Two friction stir weld samples where also provided by SKB with the labels “Corrosion KL059-COR1/T” and “KL059-COR2/T”. The samples where cut parallel to the weld on both sides (Figure 2-2).

All samples where wet polished to a 5 µm surface finish using a series of SiC grinding paper and diamond paste for the final polishing step to achieve a surface finish of 1 µm. After polishing, the samples where degreased in Acetone, Toluene and Ethanol and washed in ultrapure water and stored in a desicator prior to further use.

Table 2-1. Overview of samples.

Sample marking	Position	Comment
L006	170°	Root fault in weld
L015	15°	
L017	43°	
L019	343°	
L013		

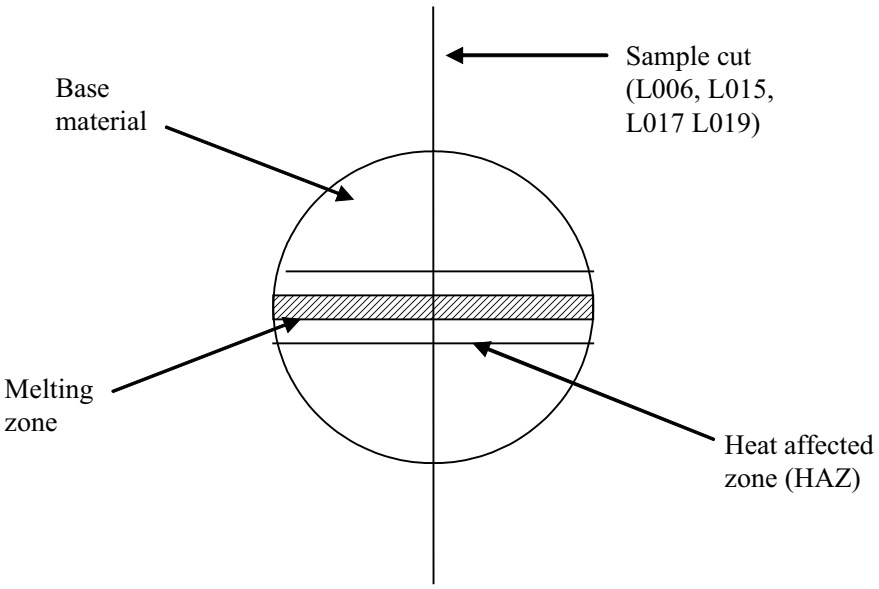

Figure 2-1. *Sample preparation.*

Figure 2-2. *Friction stir weld sample. The centerpiece contains the weld in the upper half of the sample.*

2.2 Scanning Kelvin Probe

The vibrating capacitor or Kelvin technique, which has been used for a long time to measure the work function or contact potential of metals in vacuum or in gases and to study the adsorption of species on the surfaces of metals, has been adapted to the measurement of corrosion potential. Stratmann and his co-workers have applied Kelvin probe method to study the atmospheric corrosion of metals covered with thin electrolyte layers /7, 8, 9/. In 1991, a scanning Kelvin microprobe system was described. Since then, the Scanning Kelvin Probe Microscope (SKPM) has been successfully used in corrosion science, especially for mapping the potential distribution under organic coatings. Figure 2-3 shows an experimental setup of a scanning Kelvin probe. A motorized X-Y stage controlled through a microcomputer is used to scan over the specimen. The KP potential is measured through an electronic feedback system that uses the ac signal from the working electrode as a driving force for the control circuit. The ac signal is first amplified and then sent to the lock-in amplifier. The output of the lock-in amplifier is then used to adjust a battery applied between the probe and the sample. Until the null condition is reached, the data are sent to the computer for display and analysis.

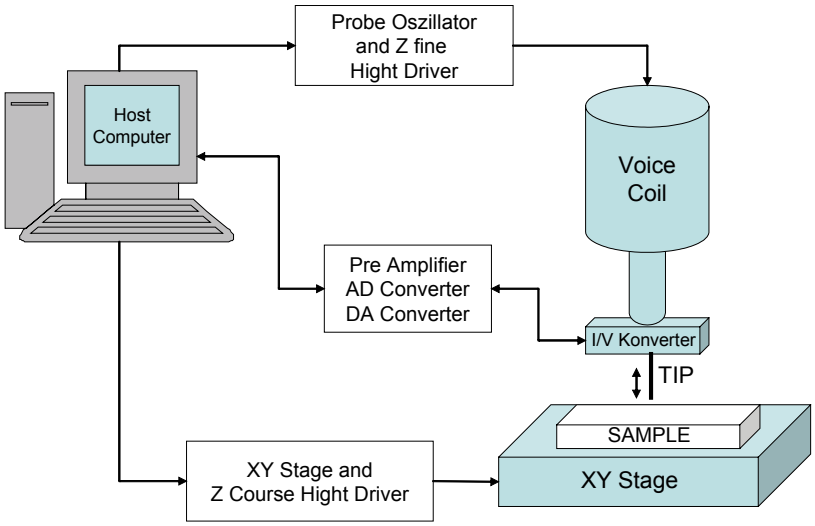

Figure 2-3. *Scanning Kelvin probe principle.*

2.3 Microscopy

2.3.1 Light microscopy

Two light microscopes where used to analyze the samples:

1. Stereomicroscope Leica MZ6 (0.63–4.00 lens) fitted with Sony Exwave HAD color video camera. Images where acquired using Easy Measurement 2000 software version 2.4.1.0 (Bergström Instrument AB, Solna, SE).
2. Metallurgical Microscope Nikon Epiphot-TME fitted with same camera as above. The same imaging software was used to acquire images.

2.3.2 Atomic force microscopy

The Atomic Force Microscope (AFM) is being used to solve processing and materials problems in a wide range of technologies affecting the electronics, telecommunications, biological, chemical, automotive, aerospace, and energy industries. Atomic Force Microscopes (AFMs) are capable of generating 3D images of surface topography with nanometer resolution. This powerful technology allows material scientists new insight into the diversity of microstructures and defect properties. Application of AFM to metallographic specimens allows quick and easy generation and quantification of images in the nanometer range. AFM studies where performed with an AutoProbe M5 system (Veeco, USA) Temperature (23°C ± 1°C) and relative humidity (50% ± 5%) were controlled during imaging. AFM Scanning tips where non-contact Ultralever, supplied by Veeco, USA.

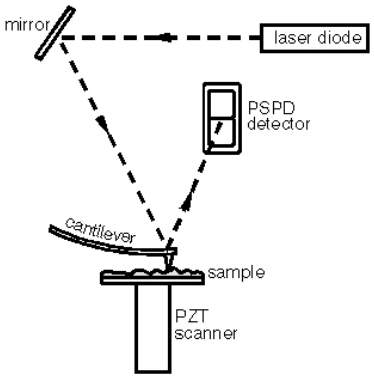

Figure 2-4. *AFM Principle.*

2.4 Autoclave

A schematic outline of the autoclave is shown in Figure 2-5. All parts of the autoclave vessel that come in touch with the liquid are made of Hastelloy C-276 nickel base alloy. The autoclave vessel inner diameter is 176 mm and the inner length is 318 mm, resulting in a total empty volume of 7.7 litres. The maximum allowed pressure is 50 bar and maximum allowed temperature is 250°C. A high pressure pump with an adjustable flow between 0 and 20.2 litre per hour is used for liquid circulation. Two storage tanks for liquids with a volume of approximately 27 litres each are fitted under the autoclave, see Figure 2-5 and 2-6. During a test run liquid is taken from one of the storage tanks and pumped into the bottom of the autoclave vessel after passing an electrical pre-heater. A 4.5 kW electrical element wrapped around the whole body heats the autoclave mantle. After the liquid has passed the autoclave it continues through a cooler, through a particle filter, a pressure regulator and back to one of the storage tanks.

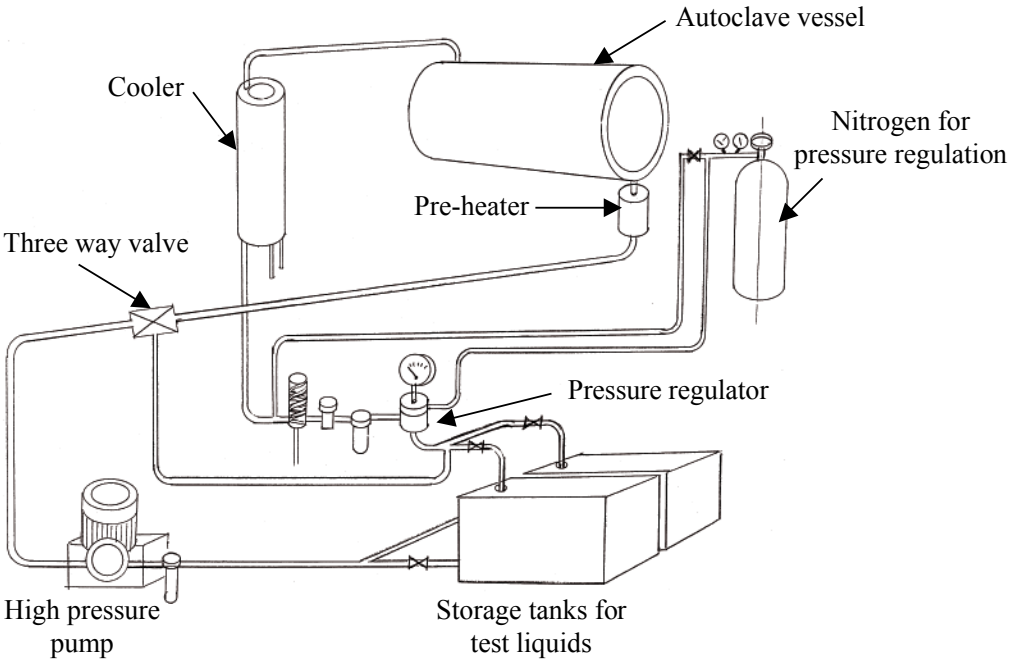

Figure 2-5. *Outline of the autoclave design.*

Figure 2-6. *Picture of autoclave table with liquid storage tanks and the high pressure pump.*

2.5 Test solution and conditions

Experiment 1

Air saturated 1% NH_4OH solution, 80°C, 10 bar, 16 days.

Experiment 2

Air saturated Sodium Citrate solution: 1 M HCl, 0.25 M trisodiumcitrate, 0.015 M CuCl, pH 4.0 (adjusted with HCl), 80°C, 10 bar, 7 days.

3 Results and discussion

3.1 Scanning Kelvin Probe

Surface potential measurements were taken from the longitudinal cut cylindrical sample L019 and from the disk sample (L013). For this purpose, samples where polished to a 1 µm surface finish using successive wet polishing steps as described in Section 2.1.

It should be noted that the image shown in Figure 3-2 was chosen to visualize the area investigated with SKP and was not the sample that was investigated.

It was observed that the surface potential of the weld and heat effected zone is ca 200 mV more anodic compared to the base material. It can also be noted that the base material has a slightly more noble potential compared to the lid material.

It can be noticed in this figure that where the canister material and the lid material join, a strong anodic potential was measured (ca 200 mV difference). At this area, the material is not welded together.

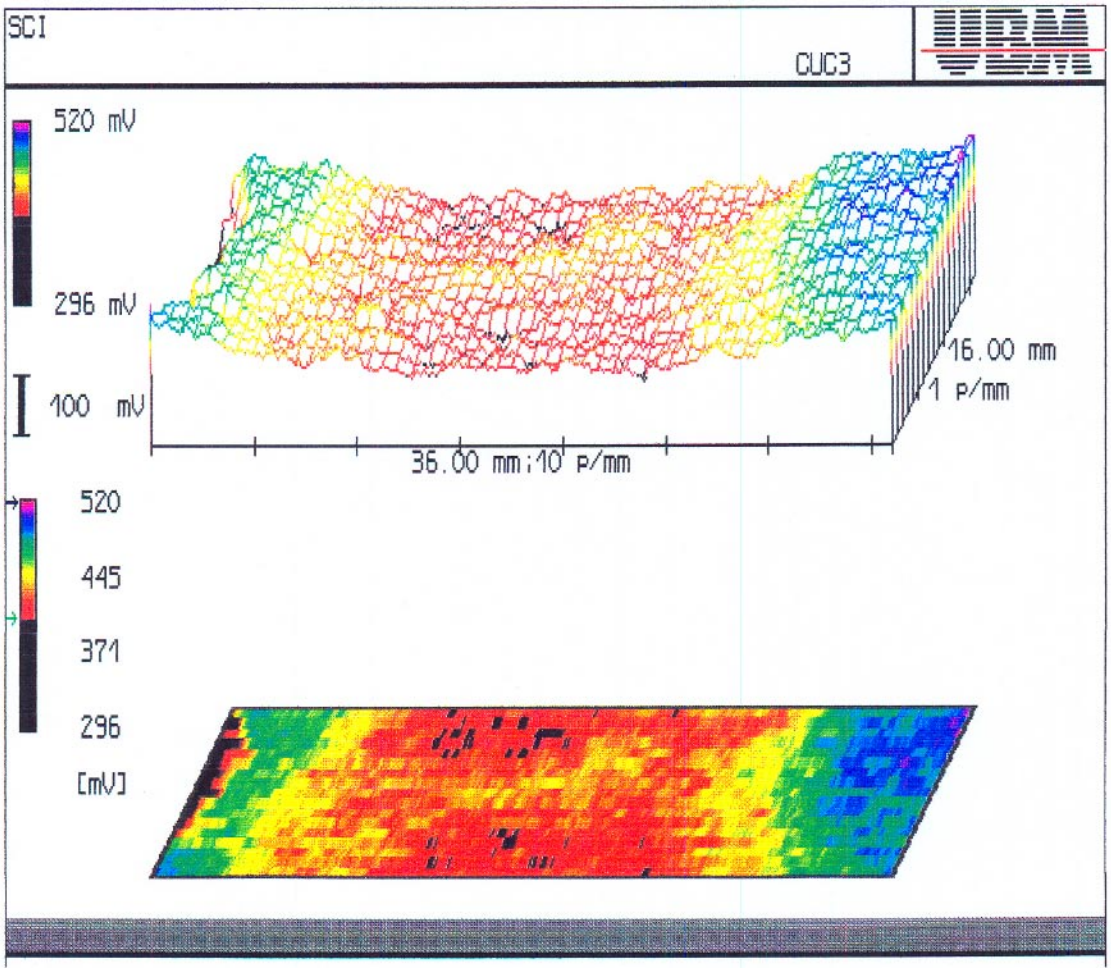

Figure 3-1. *Scanning Kelvin Probe image from sample L019. The scanned area was 36 mm wide and 16 mm deep and the offset from the making was 40 mm.*

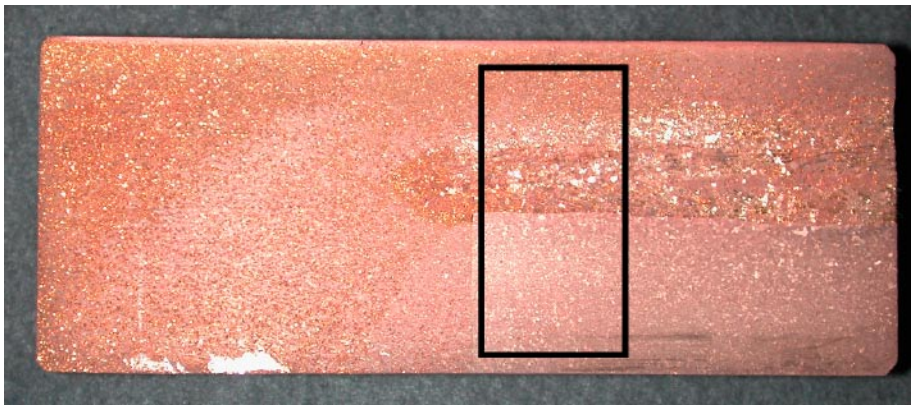

Figure 3-2. *Exposed sample revealing canister material and lid material. The marking indicates the scan area of the SKP image above, rotated 90°.*

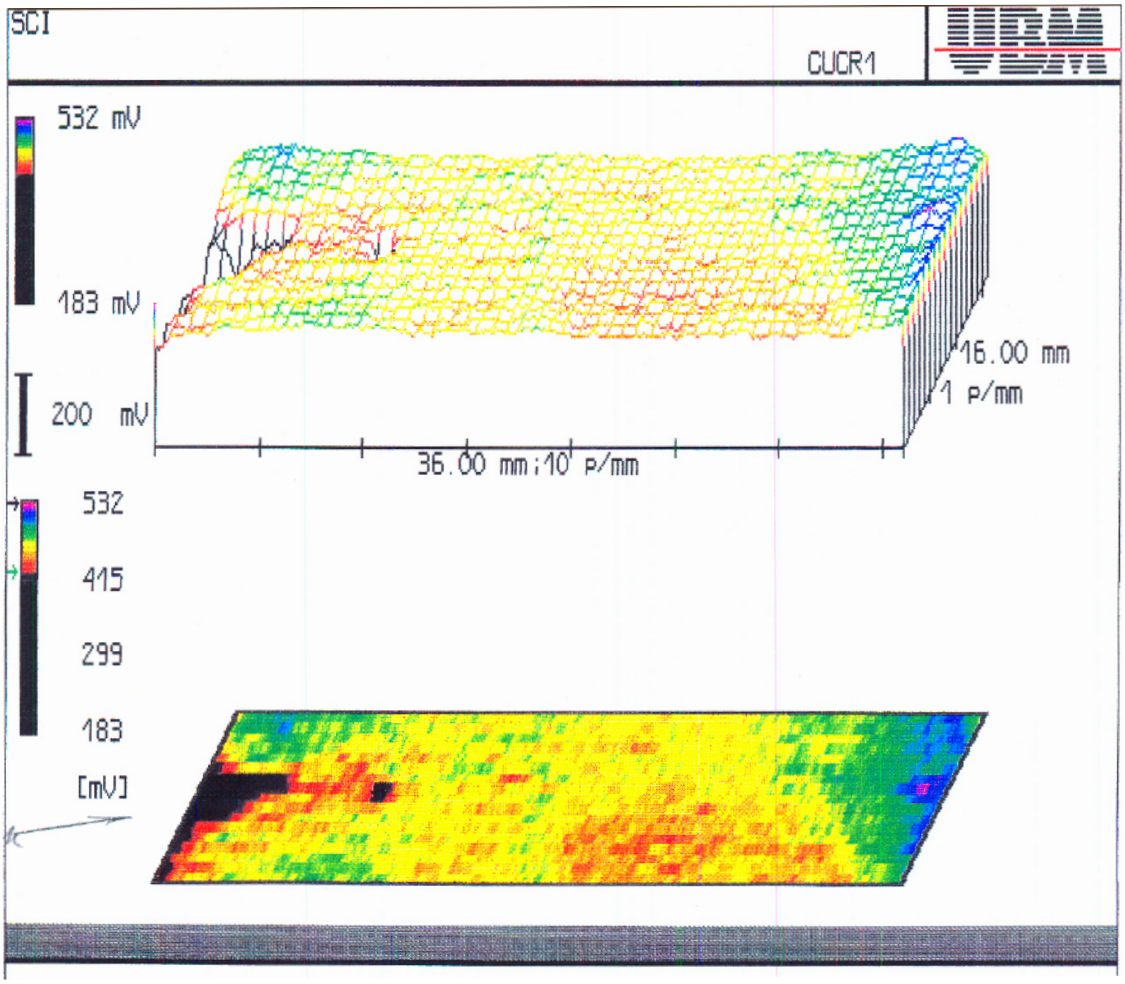

Figure 3-3. *Scanning Kelvin Probe image over the root area of the weld over the joint between the canister and its lid (sample L019).*

Inside the weld area half moon shaped anodic areas where observed (Figure 3-5). These shapes do not coincide with the grain structure of the welds.

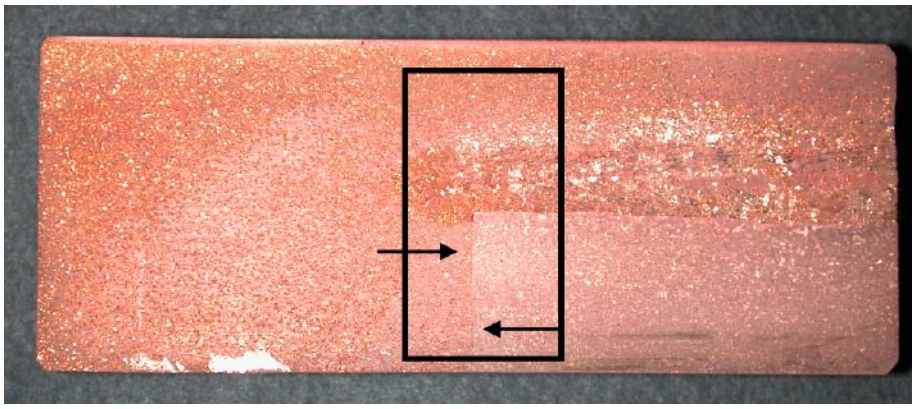

Figure 3-4. *Exposed sample revealing canister material and lid material. The marking indicates the scan area of the SKP image above, rotated 90°.*

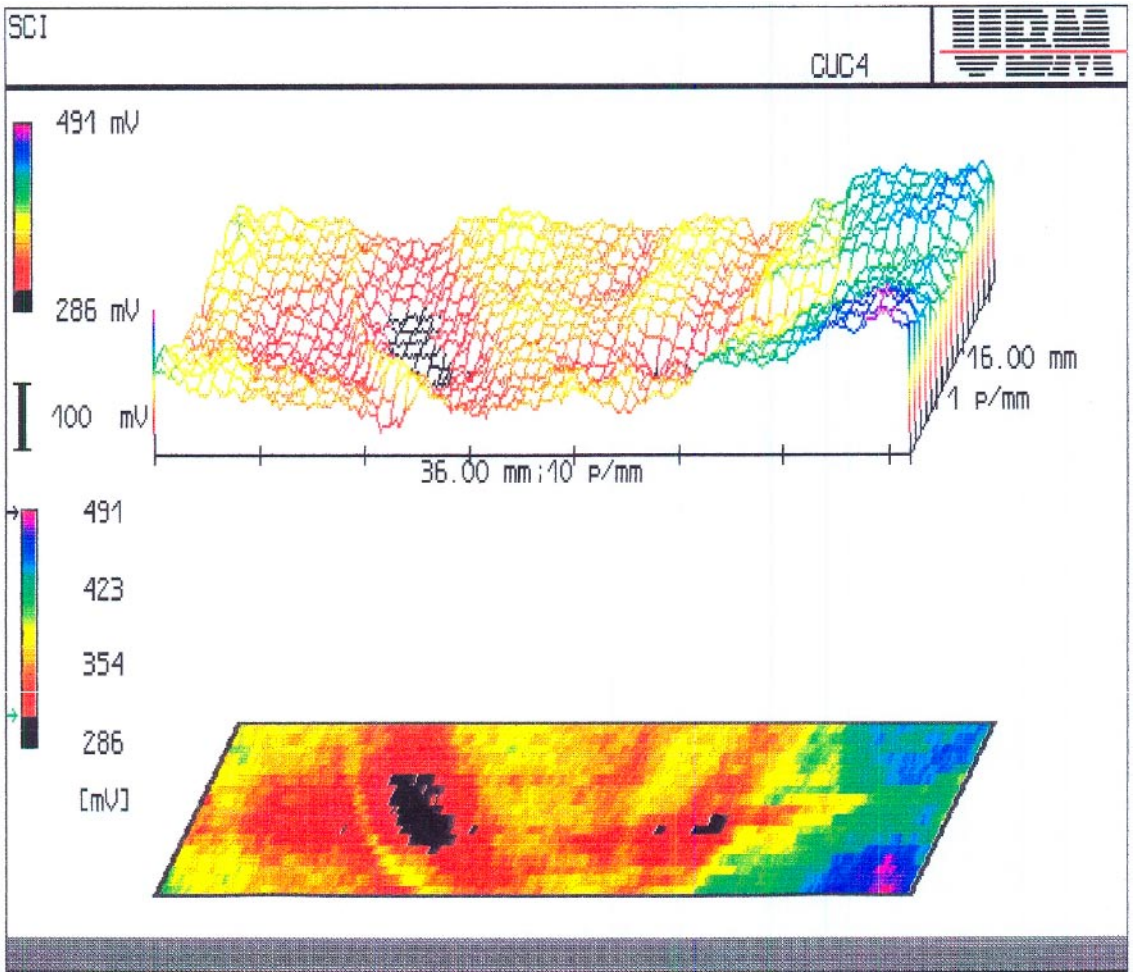

Figure 3-5. *Scanning Kelvin Probe image over the weld close to the outer side of the sample.*

The SKP image shown in Figure 3-7 indicates that the weld area is more anodic (more likely to corrode) compared with the base material from lid and cylinder by ca 100 mV. Since this is the weld surface exposed to the bentonite, such a potential difference could raise concern about galvanic corrosion of the welds.

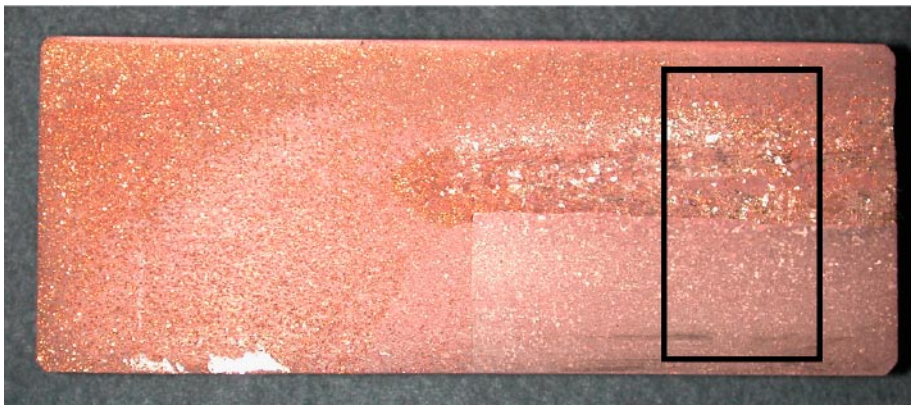

Figure 3-6. *Exposed sample revealing canister material and lid material. The marking indicates the scan area of the SKP image above, rotated 90°.*

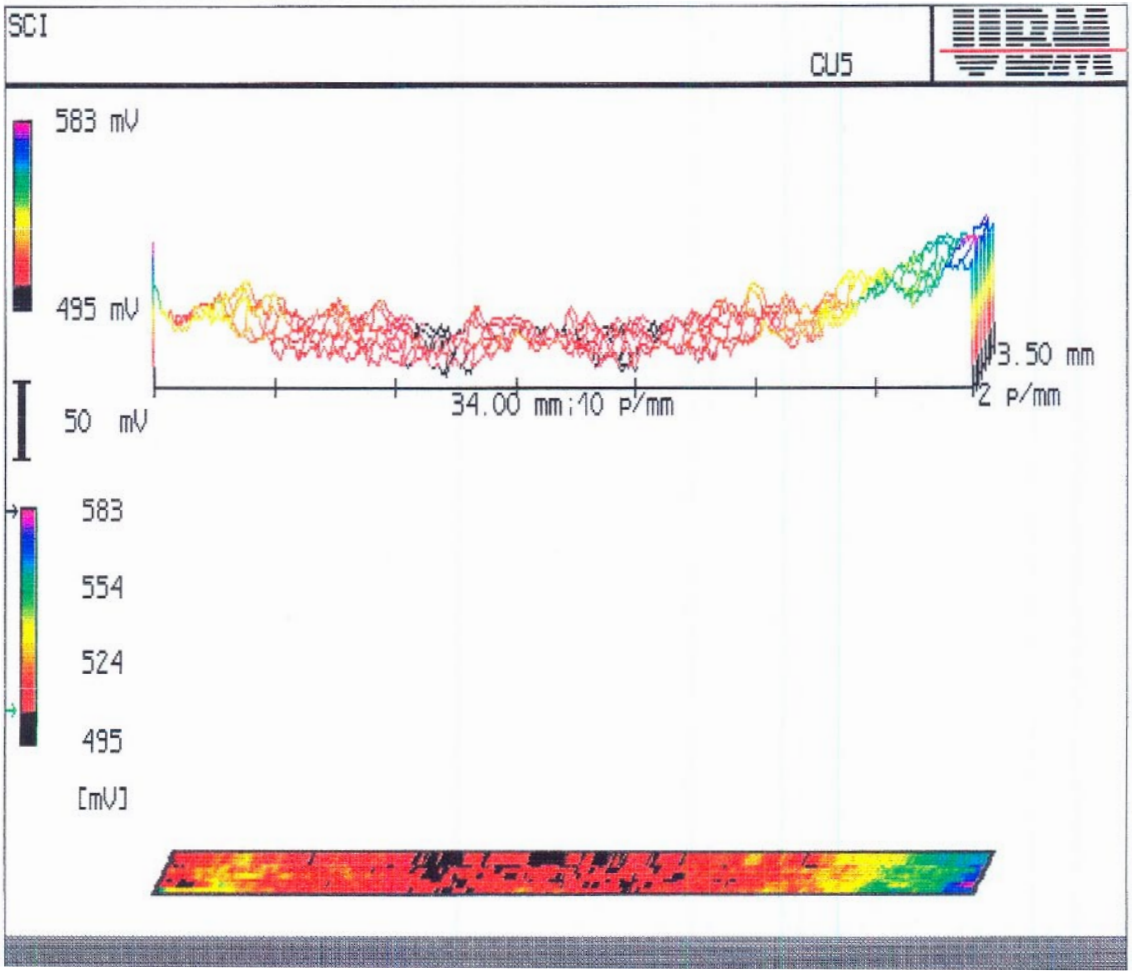

Figure 3-7. *L013 scan over weld.*

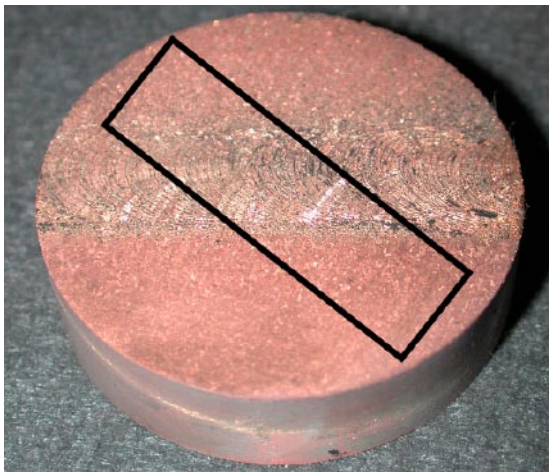

Figure 3-8. *Exposed sample L013 revealing canister material and lid material. The marking indicates the scan area of the SKP image above.*

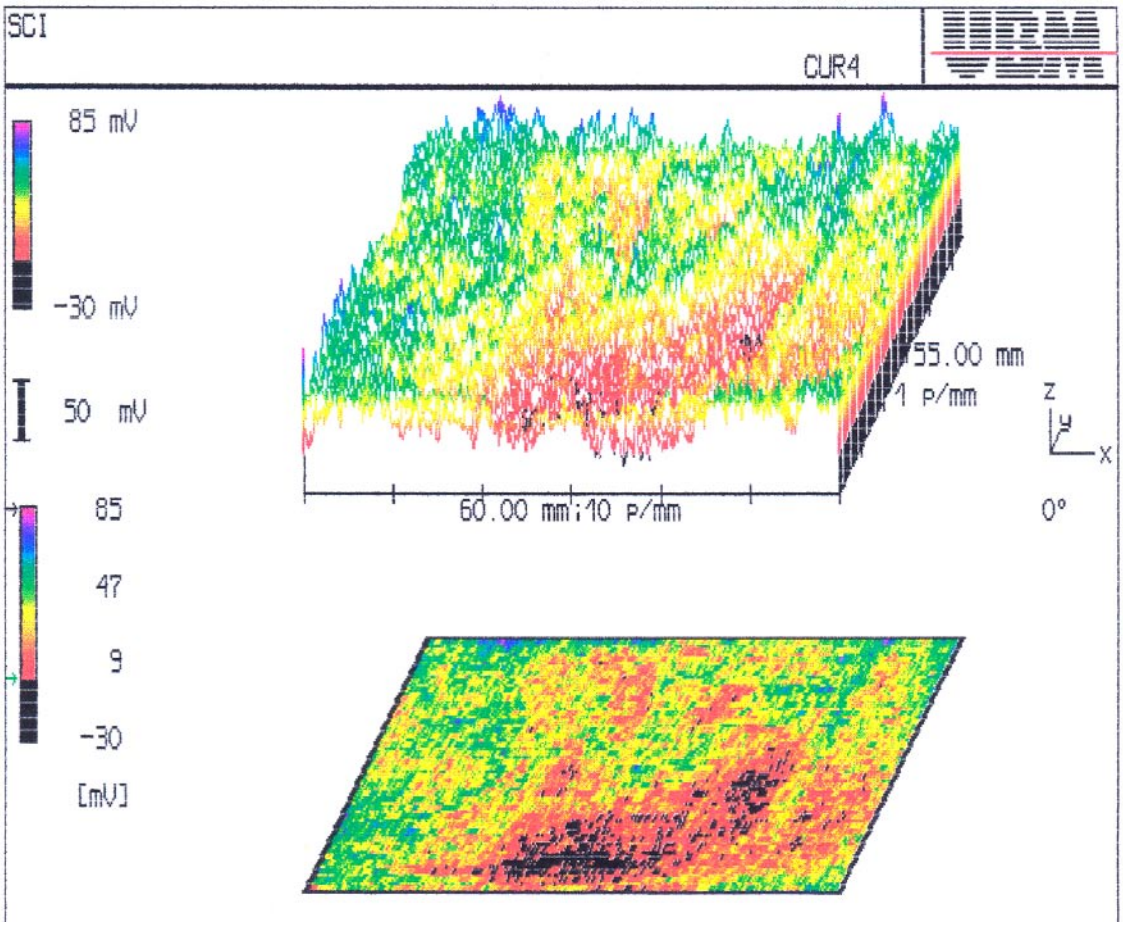

Figure 3-9. *SKP image of the friction stir weld sample "Corrosion KL059-COR1/T".*

Friction stir welding seems to reduce the potential difference between the weld and base materials. However, a potential difference of ca 75 mV was observed on the right side (exposed to the environment) between weld and base materials.

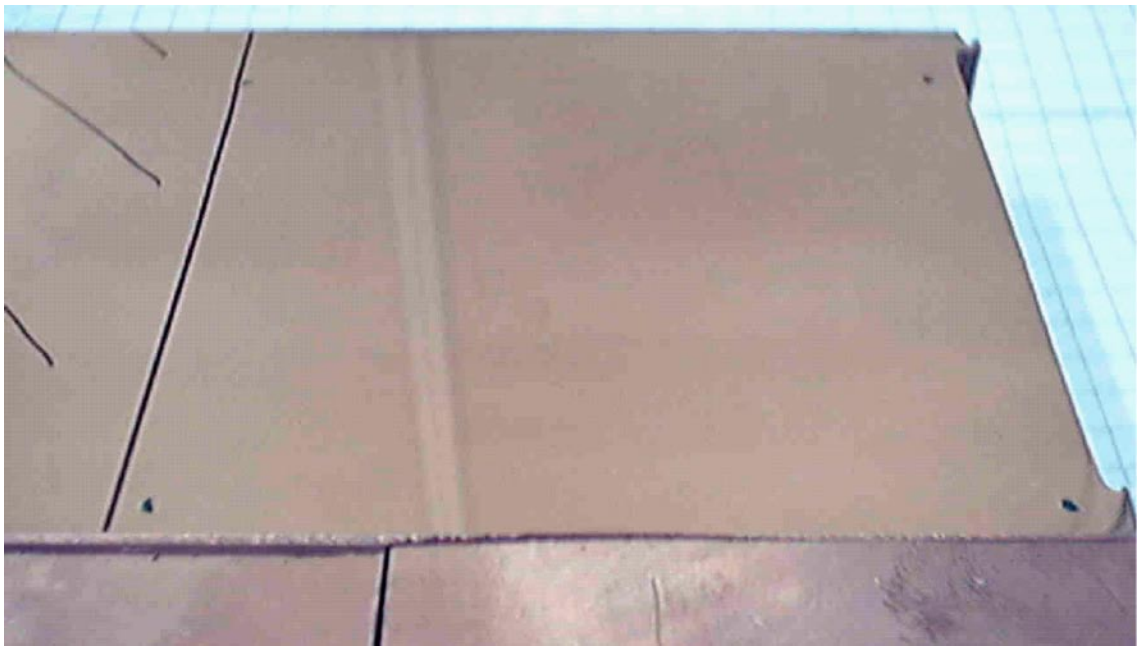

Figure 3-10. *Photograph of the sample "Corrosion KL059-COR1/T". The white lines indicate the SKP scanning area shown in Figure 3-9.*

3.2 Microscopic examinations

After each experiment, microscopic examinations of each sample were performed.

3.2.1 Experiment 1

Microscopic Images from Cu-weld samples after exposure for 16 days in air-saturated 1% NH_4Cl solution at 80 Celsius and 10 bar pressure.

The image shown in Figure 3-11 is typical for all samples. The weld area was most corroded, followed by the cylinder material and the lid material was less attacked. Furthermore, a distinct pattern for corrosion was observed in the weld area that is not coinciding with the grain structure, but rather looks like a "flow" pattern. This "flow" pattern can be better seen in the micrographs below.

Figure 3-12 shows clearly the different level of corrosion on the two types of base materials. The canister material is finer grained, while the lid material is hot forged, exhibiting larger grain sizes. However, the main corrosion attack was observed on the weld material across the grain structure.

A more detailed image to that fact is given in Figure 3-13 which provides evidence that the corrosion attack in the weld zone was mostly across grain boundaries following a stir type pattern rather than the grain structure.

Figure 3-14 to 3-16 show images from sample L013. The main corrosion attack was observed on the weld material following the "flow type pattern" as also observed for the samples cut longitudal.

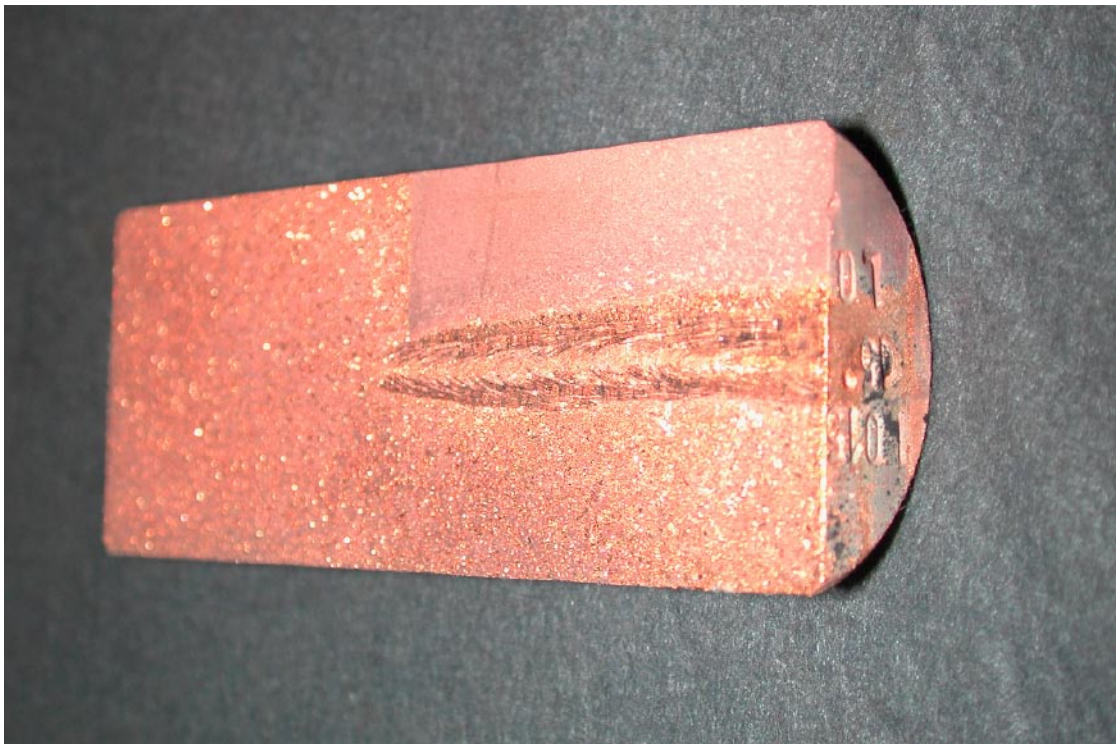

Figure 3-11. *Photograph of sample L015 (rotated 15°) after exposure, characteristic for all samples exposed.*

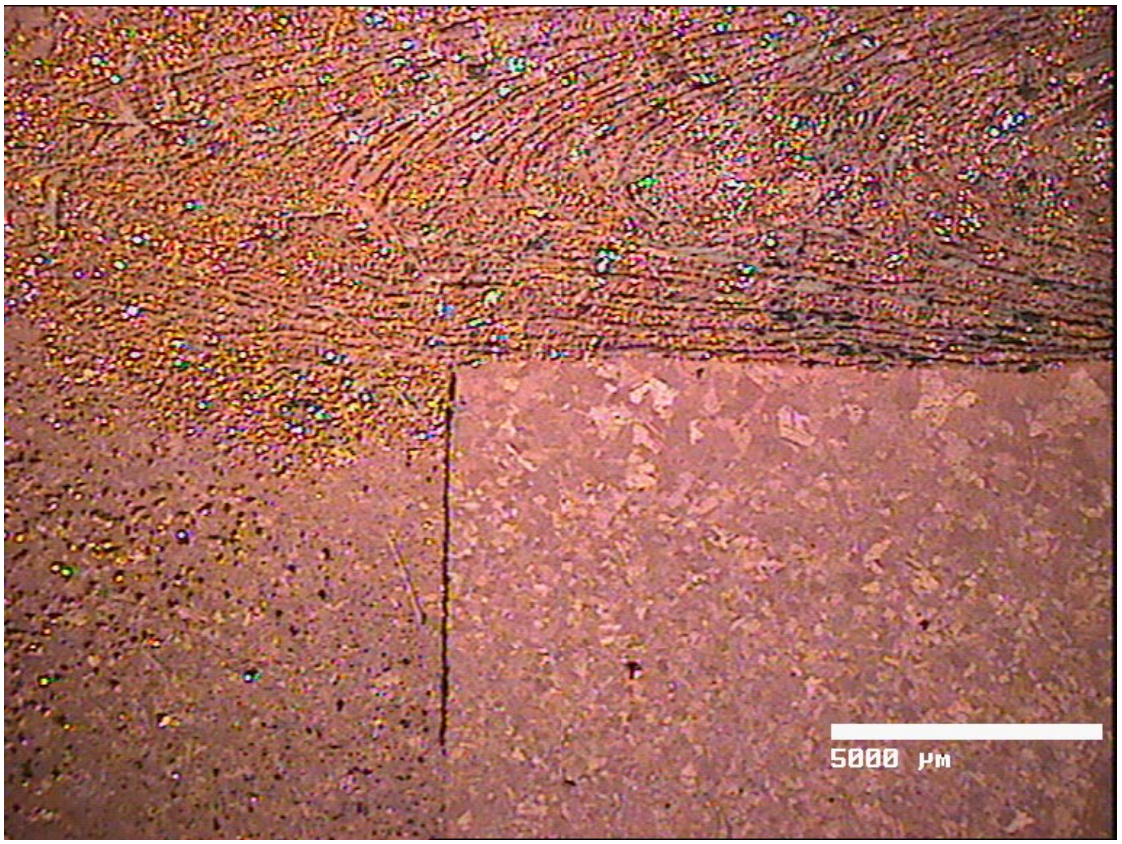

Figure 3-12. *Micrograph of sample L019. The weld area is corrode in a "flow" like pattern.*

Figure 3-13. *High magnification micrograpgh of sample L019. The grain structure can be seen but corrosion took mainly place along "markings" from the weld process rather than grain boundaries.*

Figure 3-14. *Photograph sample L013 after exposure. The grain structure is revealed along weld and markings from the welding process have been etched out of the surface.*

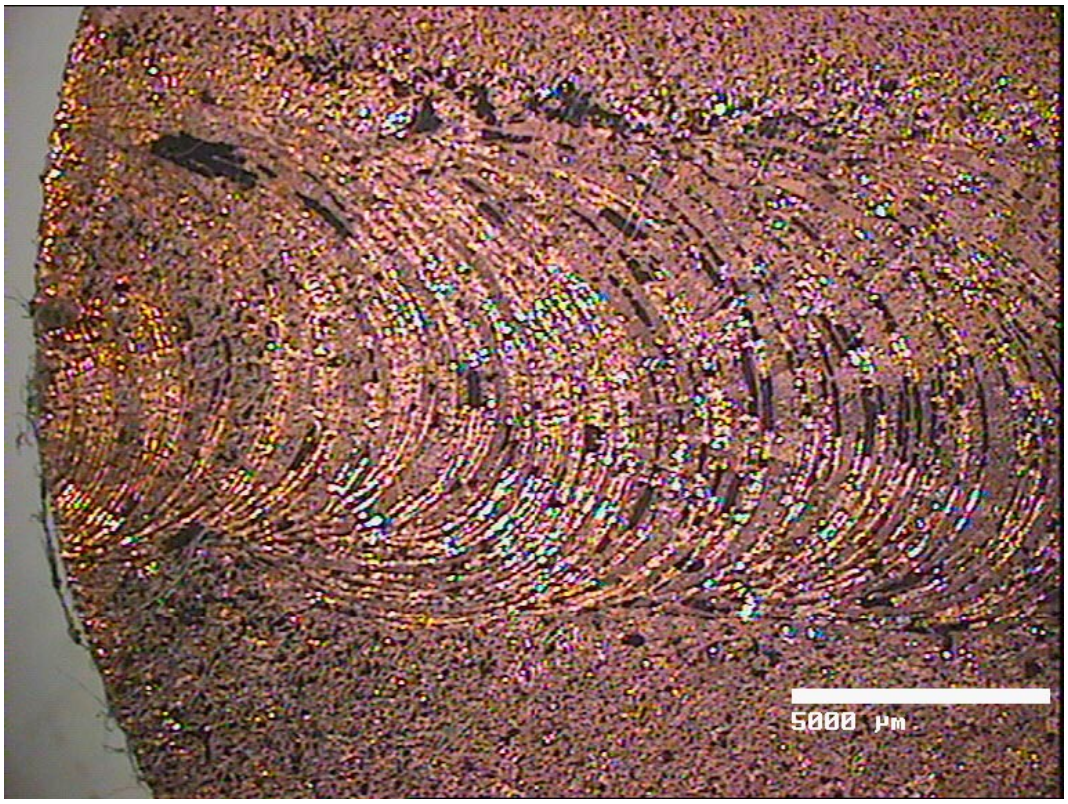

Figure 3-15. *Micrograph of sample L013. The grain structure has been revealed, but corrosion took mainly place along markings induced by the welding process. The dark areas in the image are remaining corrosion products on the surface.*

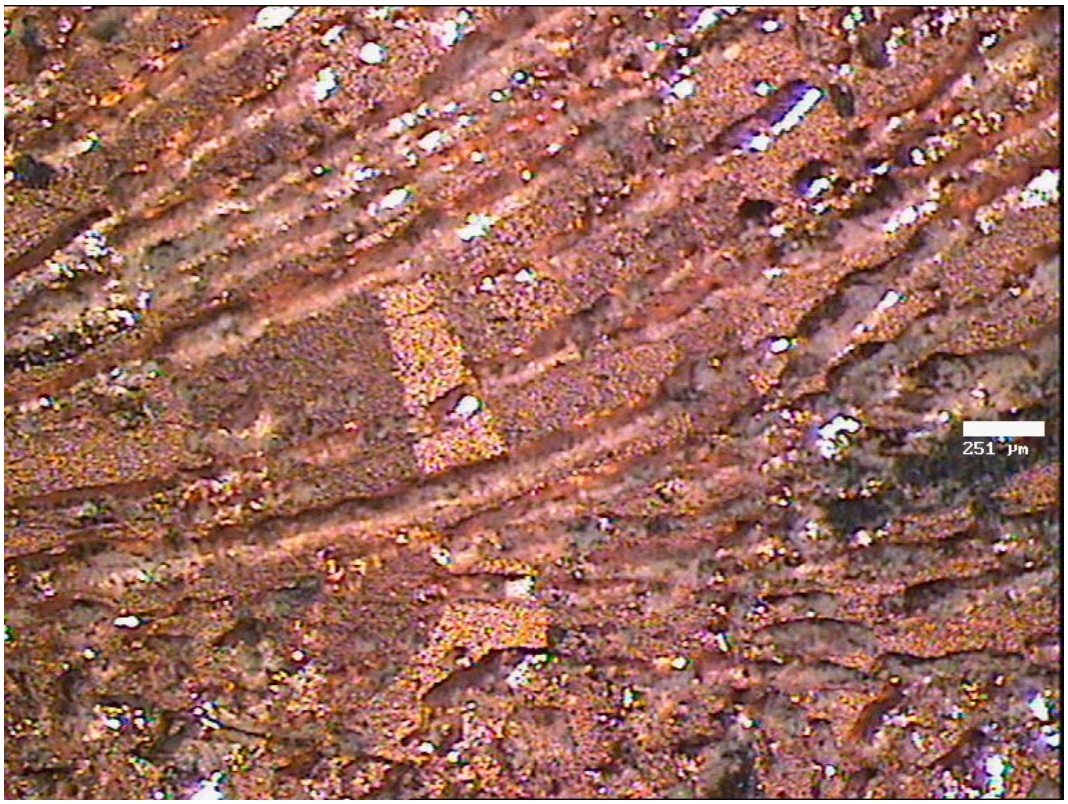

Figure 3-16. *High magnification micrograph of sample L013. It can clearly be shown that the main attack was not along the grain boundaries.*

No grain boundary corrosion could be observed in this experiment using the 1% Ammonium hydroxide solution. The solution resulted in a more general type of corrosion attack, parallel to the grain orientations. No metallic copper was found in the corrosion products recovered from the autoclave after the end of the experiment.

Since no grain boundary corrosion could be observed in this experiment, an acidified sodium citrate test solution used for inducing grain boundary corrosion in brass samples was used for the next test run. This solution has no relevance with conditions found in the repository, however, it has been shown to induce grain boundary corrosion and stress corrosion cracking of copper alloys.

Experiment 1 was only performed on electron beam welded samples.

3.2.2 Experiment 2

The images where taken after exposure to air saturated Sodium Citrate solution: 1 M NaCl, 0.25 M trisodiumcitrate, 0.015 M CuCl, pH 4.0 (adjusted with HCl), 80°C, 10 bar, for 7 days.

Figure 3-17 shows the weld root area of sample L017 after the exposure inside the autoclave. It can be noted that deep cracks have developed at the root of the weld. This is possibly due to stress corrosion induced by the residual stresses from the welding process. Furthermore, the grains show with a strong contrast in the images and corrosion attack along the grain boundaries cannot be excluded (see Figures 3-18 to 3-21).

Figure 3-17. *Micrograph of sample L017 showing a strong corrosion attack at the root the weld. Small indentions along the grain boundaries can also be observed in this sample.*

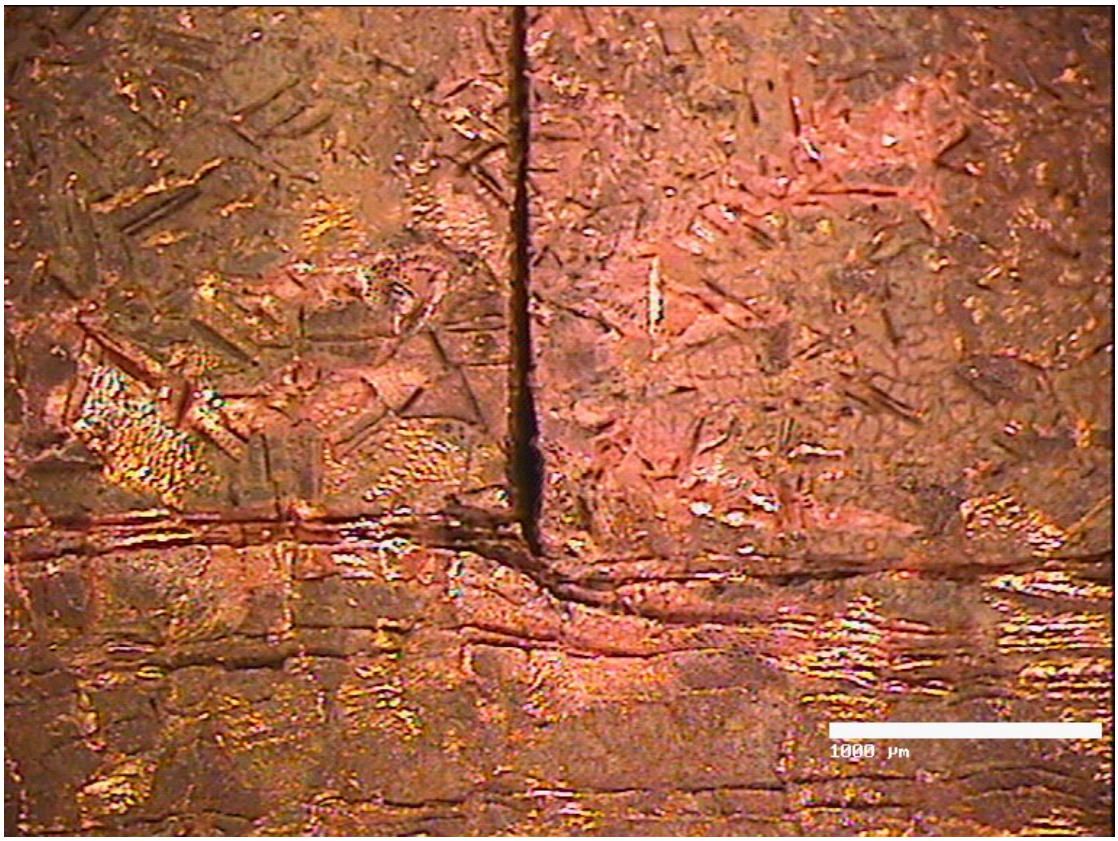

Figure 3-18. *Micrograph of sample L017 at the joint between canister and lid material.*

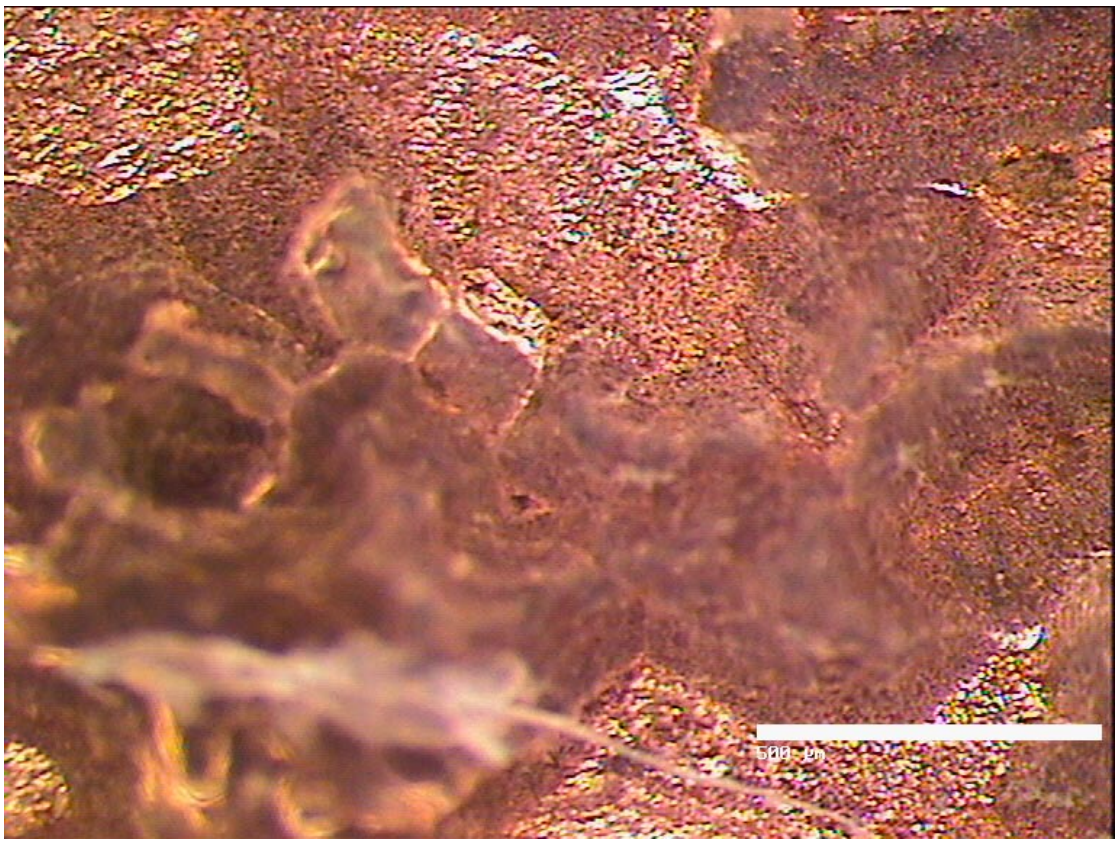

Figure 3-19. *Micrograph of sample L017. Small indentions along grain boundaries can be seen, however, this could be artifacts for shadows.*

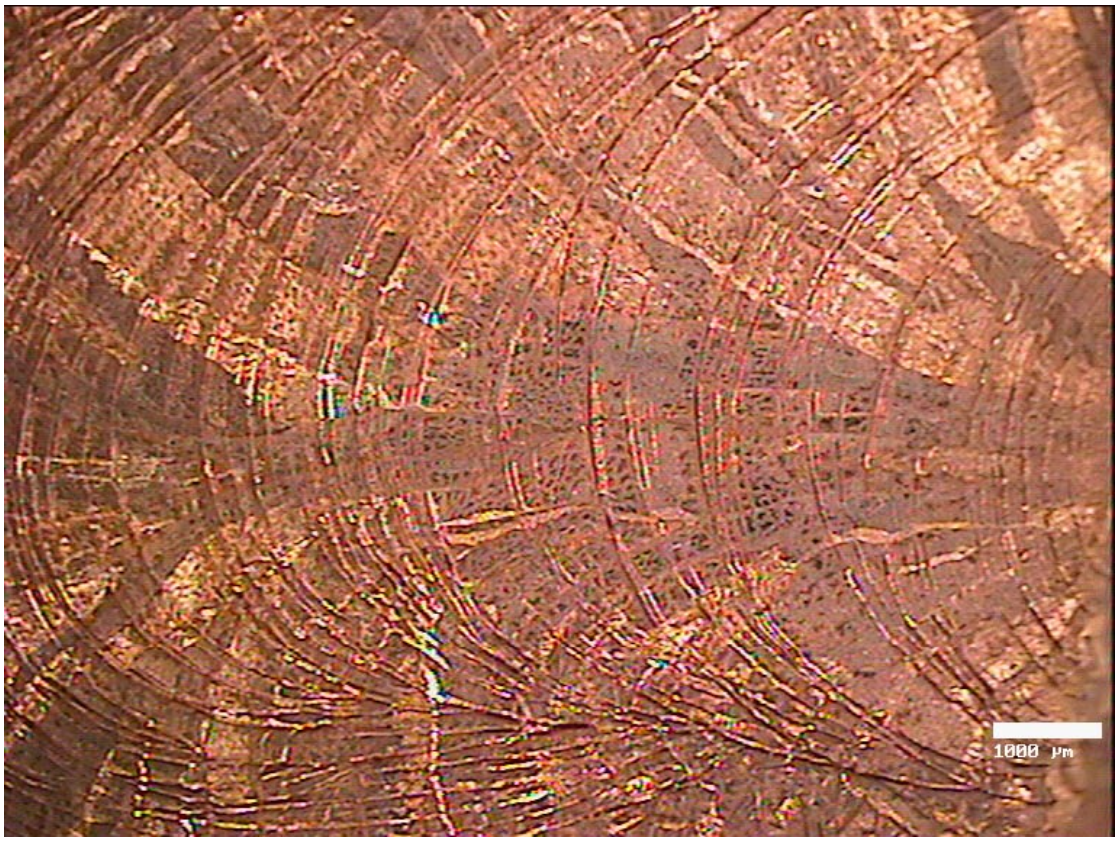

Figure 3-20. *Micrograph of sample L013 around at weld area.*

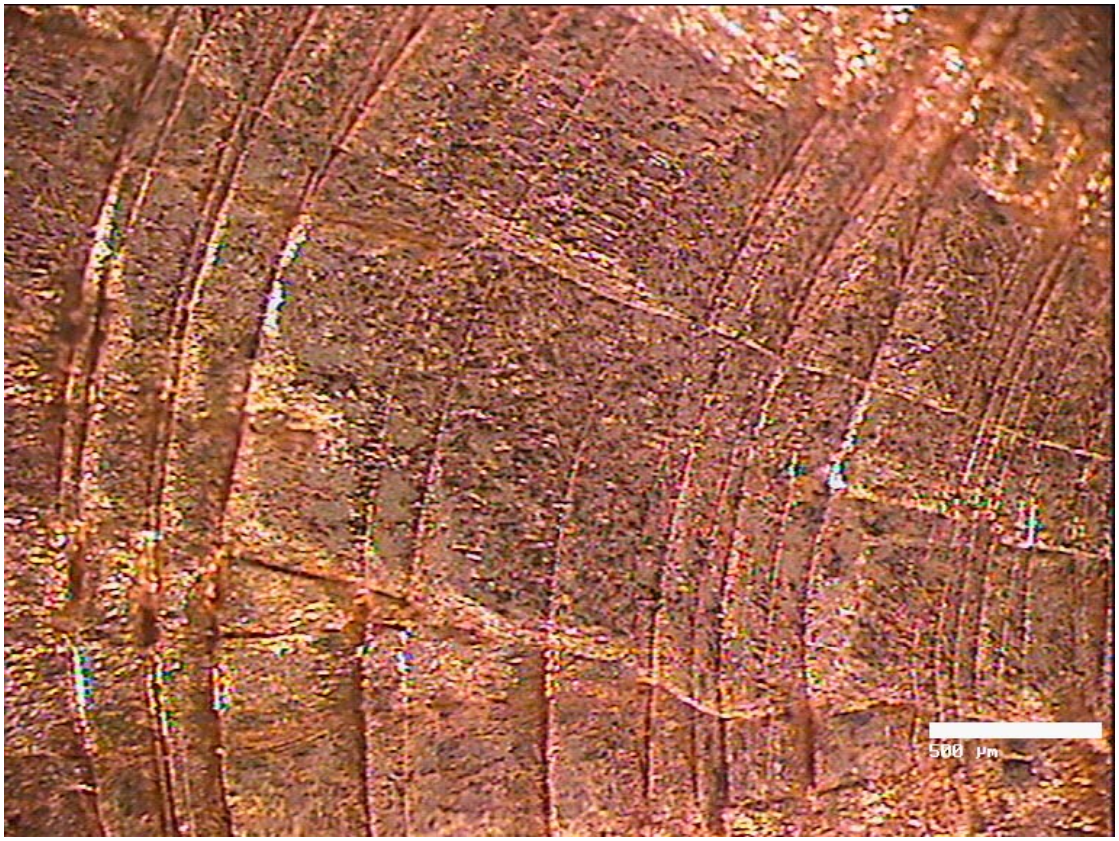

Figure 3-21. *Micrograph of sample L013 in the weld area. Shadow lines can be seen along grain boundaries.*

The conditions applied in experiment 2 were too aggressive to allow for conclusive results for proof that grain-boundary corrosion occurred, since the grains were severely attacked by the test solution. The observed lines along the grain boundaries could be shadows of the light due to height steps between grains that corroded at different angels. Therefore, a new sample cut from L013 (round sample) was polished and immersed in the test solution at room temperature for 2 hours in order to observe the onset of corrosion in the Atomic Force Microscope.

After this short exposure time, the “flow” type pattern was already etched into the surface of the weld material. It can also be noted that the grains pattern is revealed due to different coloring (oxide layers and corrosion attack) of the surface.

It was noticed that after the short exposure period, the surface it etched and revels the grain structure of the weld, heat affected zone and base material. The lid material is shown in the upper half of the image (Figure 3-22). Figures 3-23 and 3-24 show images at higher magnification of the weld area shown in Figure 3-22. Small lines along the grain boundaries have formed, indicating the onset of grain boundary corrosion. To clarify whether grain boundary corrosion occurred, the sample was placed into an Atomic Force Microscope to obtain 3D images of the surface.

Figure 3-25 shows an atomic force micrograph taken in the weld area across two grains. It can be noticed that on one grain a general type of corrosion attack has started, while the other grain clearly still shows the polishing marks. It can also be seen that the grain boundary is revealed by a thin line between the grains. Thus, grain boundary corrosion was observed using the sodium citrate solution.

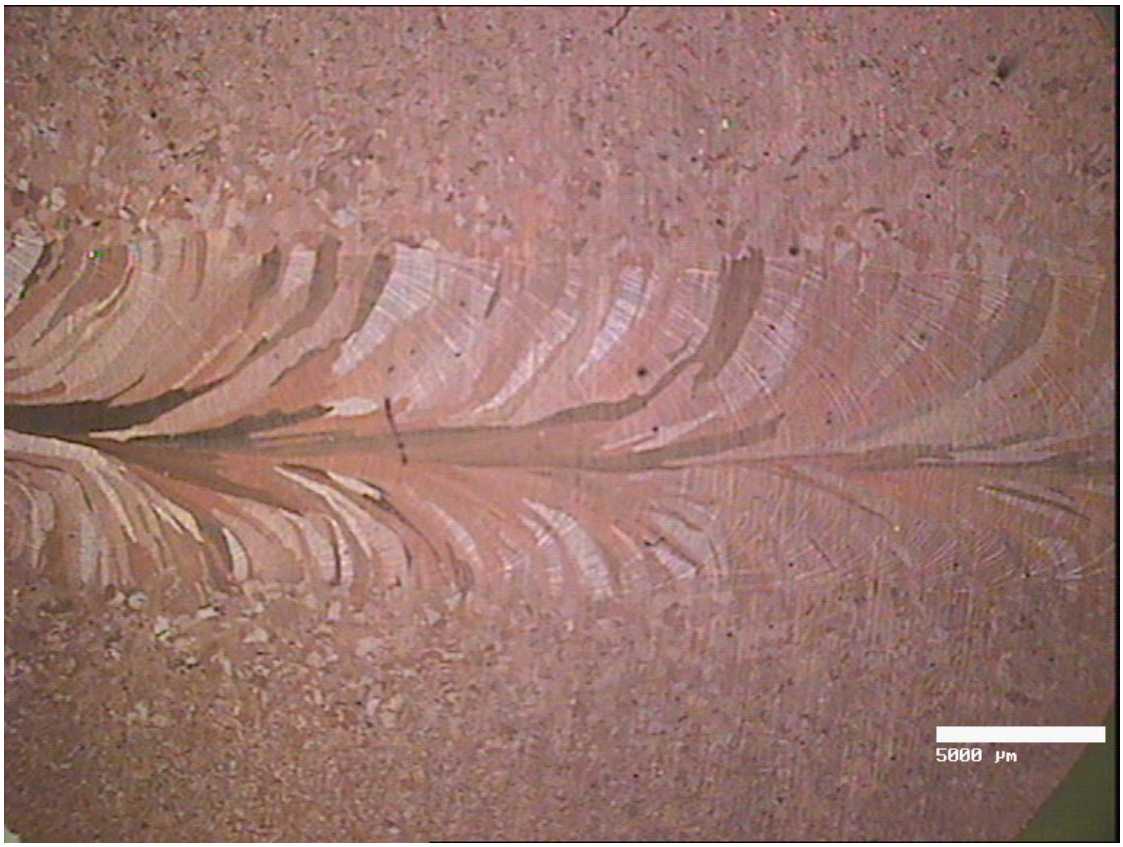

Figure 3-22. *Light micrograph of sample L013 immersed for 2 hours in the sodium citrate solution at room temperature.*

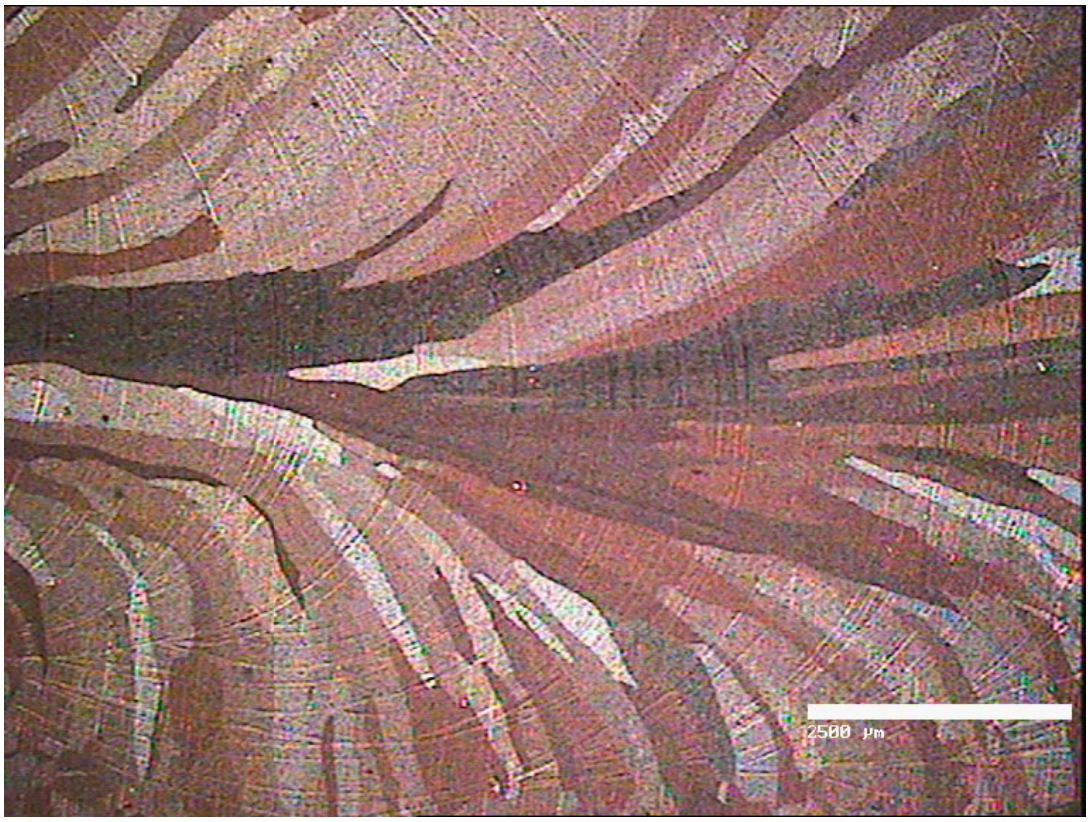

Figure 3-23. *Light micrograph of the weld area of sample L013 immersed for 2 hours in the sodium citrate solution at room temperature.*

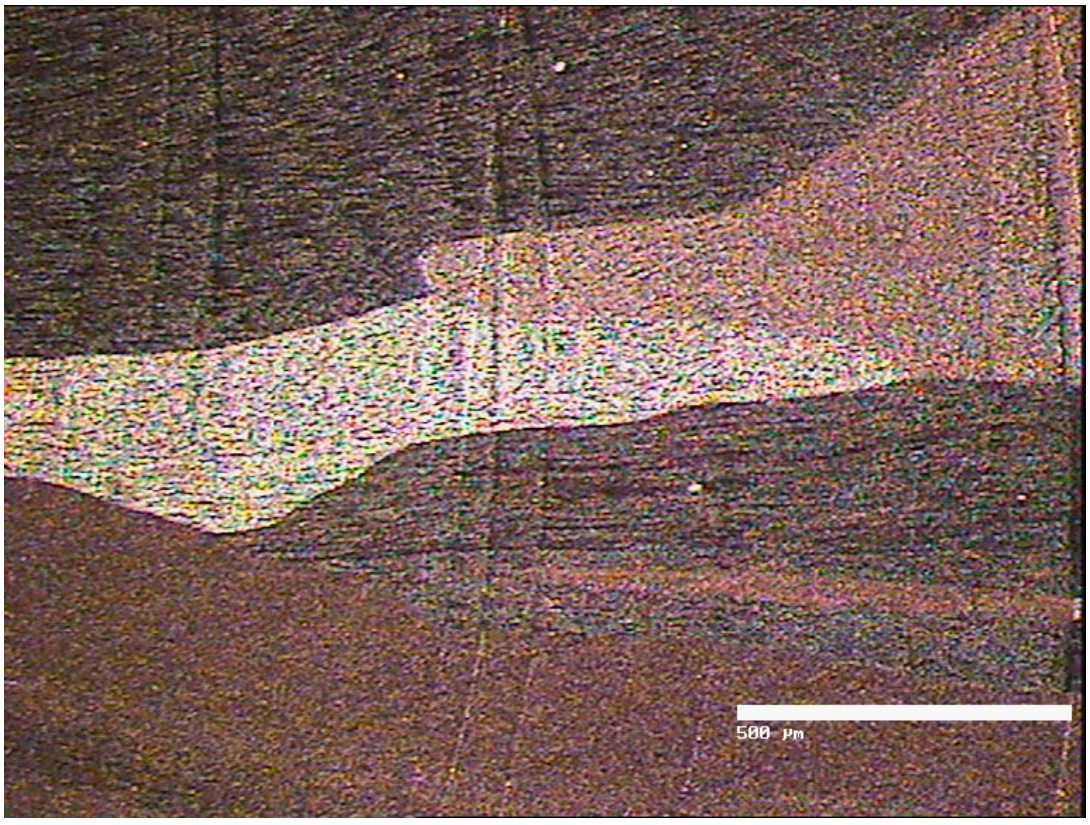

Figure 3-24. *Light micrograph of the weld area at large magnification of sample L013 immersed for 2 hours in the sodium citrate solution at room temperature.*

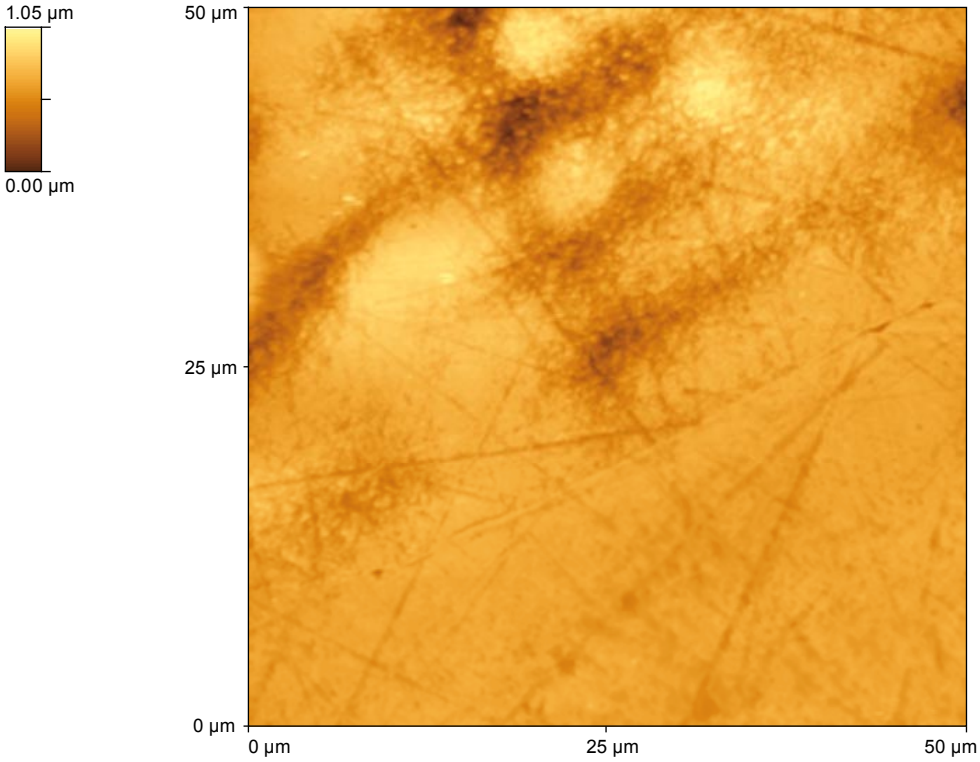

Figure 3-25. *Atomic Force Microcope image of sample L013 in the weld area across two grains.*

Figures 3-26 and 3-27 show the borders between three grains located in the heat affected zone that have been attacked by the test solution. The attack in the grain boundaries was most predominant in the heat affected zone, but could also be observed on the base material (Figures 3-29 and 3-30). Figure 3-28 shows the analysis of the depth of the grain boundary attack, clearly indicating that the lines seen in the light micrographs at the grain boundaries are indeed induced corrosion of the boundaries, rather then being artifacts.

Friction stir welded samples where exposed to the same sodium citrate solution under the same conditions at room temperature. The first observation made was that it took 20 hours before the grain structure was properly revealed, indicating a better corrosion resistance of the friction stirred samples compared to the electron beam welded samples. Light microscopic examination (Figures 3-31 to 3-33) shows clearly much smaller grains in the weld zone compared to electron beam welded samples (e.g. Figures 3-23 and 3-24).

A certain grain growth (ca with a factor of 3) could be observed between the weld root area (Figure 3-31) compared to the outer part of the material (Figure 3-33). Figure 3-32 shows a defect in form of a crack in the weld (white arrow).

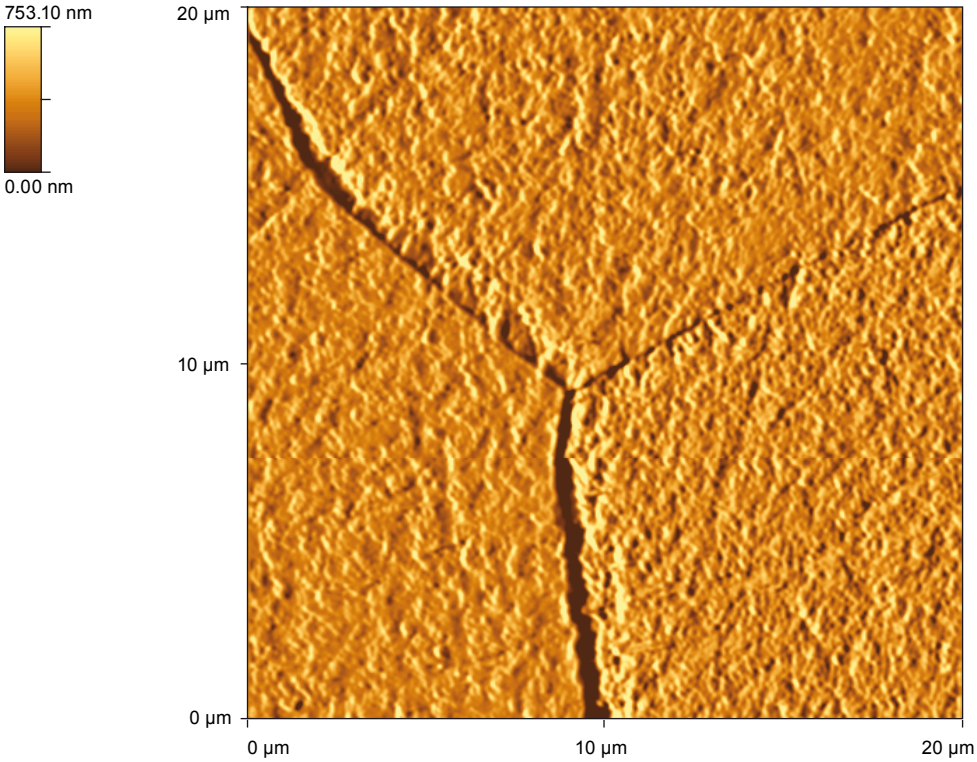

Figure 3-26. *Atomic Force Micrograph of sample L013 in the heat affected zone across three grains. The image has been "shaded" to allow better contrast.*

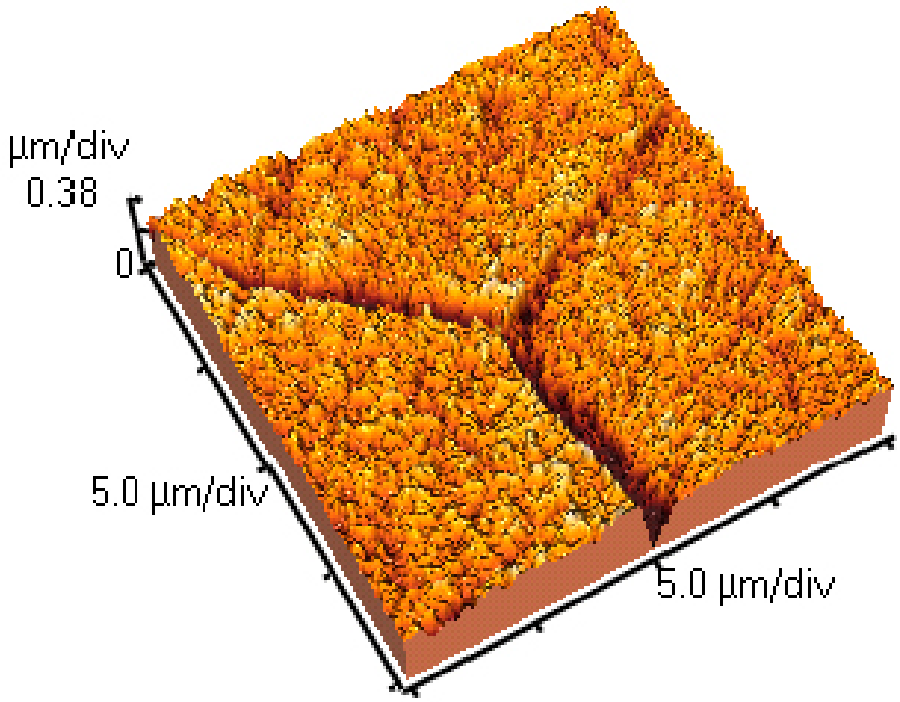

Figure 3-27. *3D image of the Atomic Force Micrograph presented in Figure 3-23.*

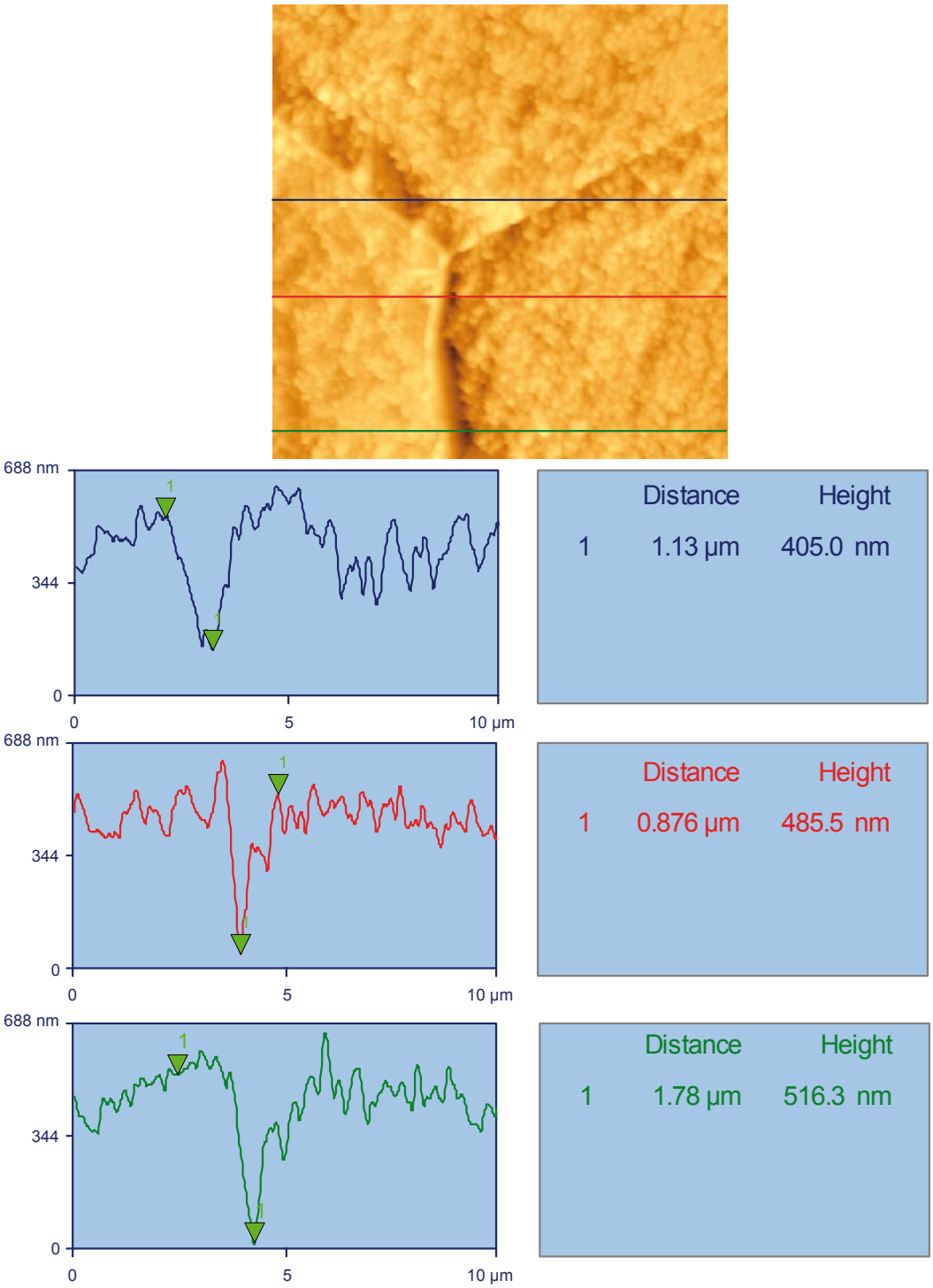

Figure 3-28. *Measurement of grain boundary corrosion depth of the Atomic Force Micrograph show in Figures 3-23 and 3-24.*

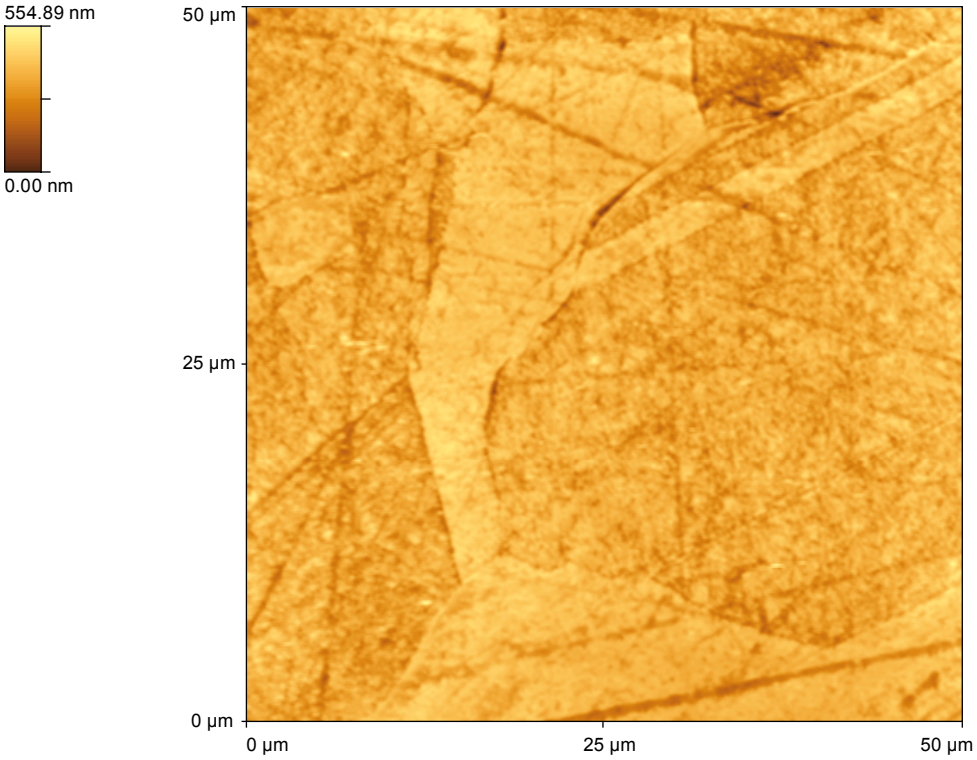

Figure 3-29. *Atomic Force Micrograph of sample L013 taken on the base material.*

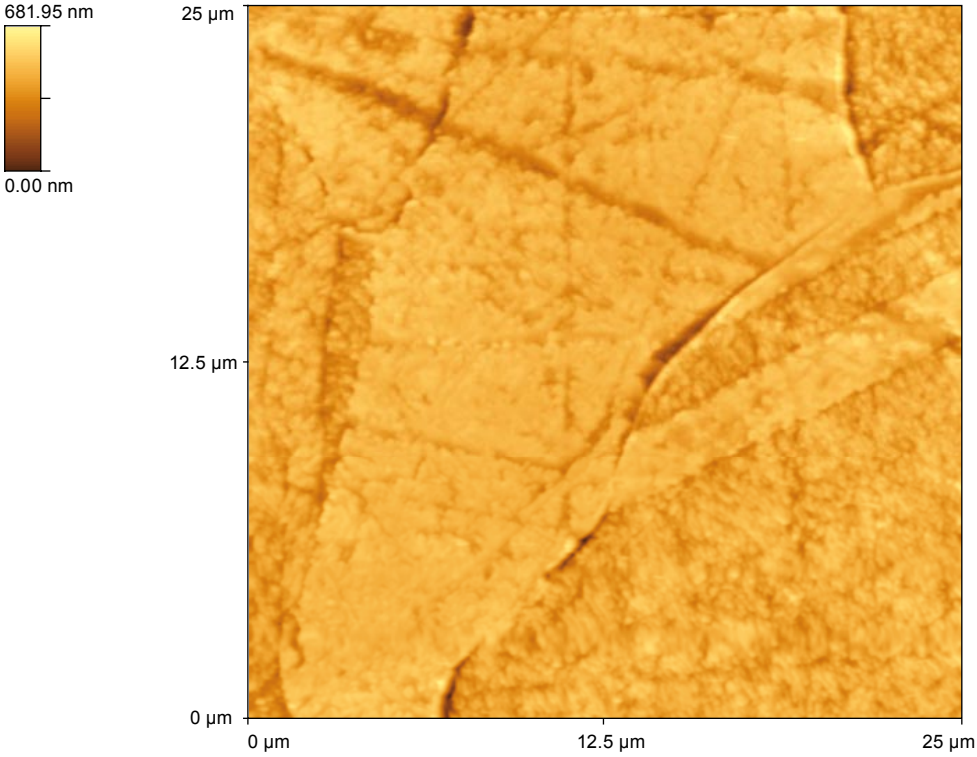

Figure 3-30. *Higer magnification the Atomic Force Micrograph shown in Figure 3-26.*

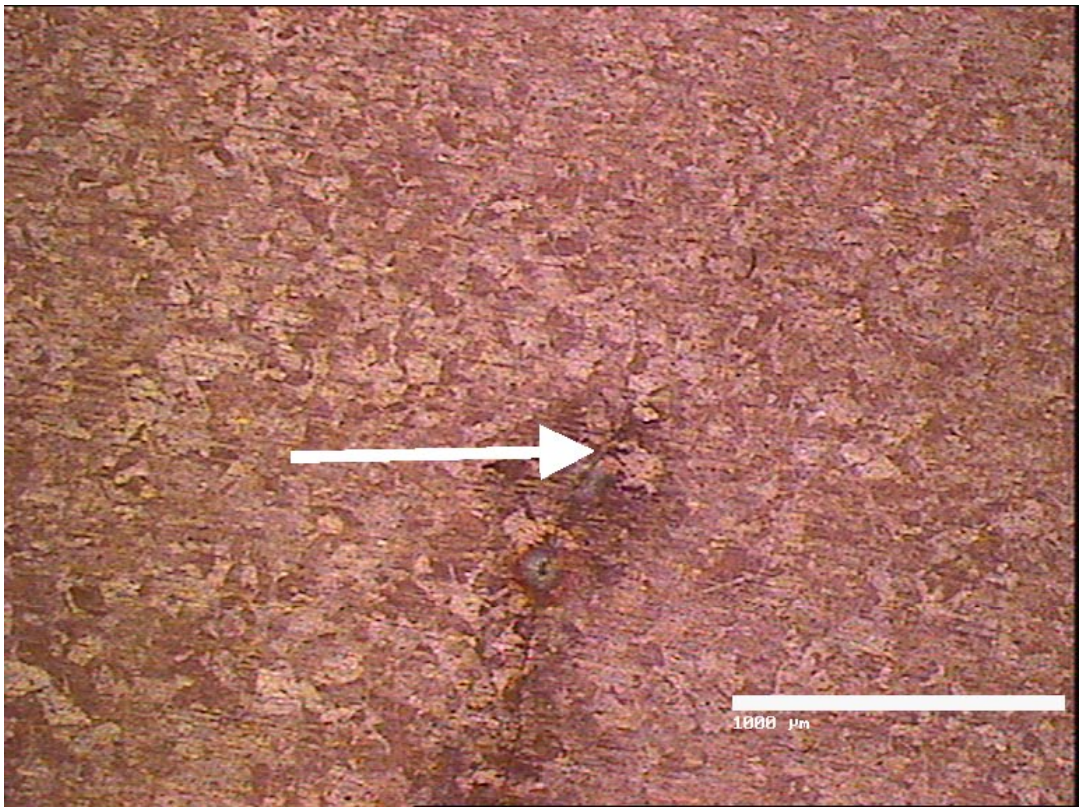

Figure 3-31. *Light micrograph taken at the weld root of the friction stirred sample. The arrow indicates the start of the fusion zone.*

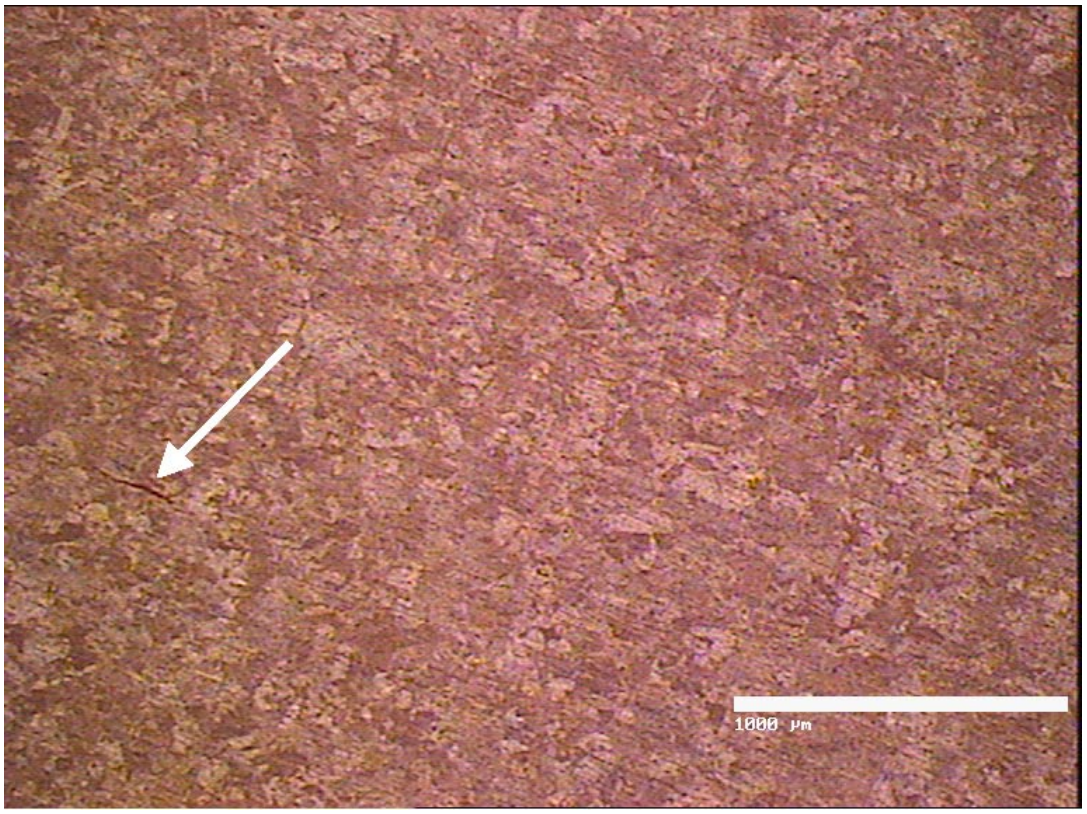

Figure 3-32. *Light micrograph taken at the weld zone of the friction stirred sample. The arrow indicates a crack in the material.*

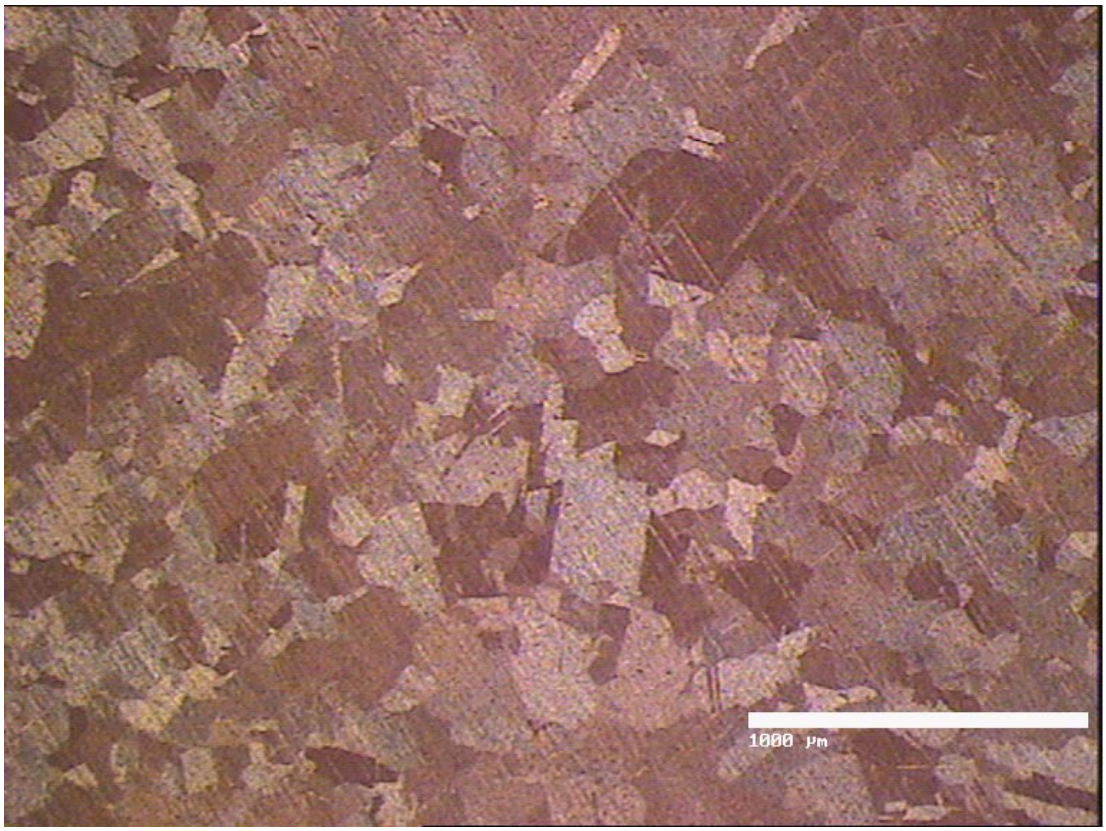

Figure 3-33. *Light micrograph taken at the weld zone of the friction stirred sample close to the outer side that will be exposed to the environment. It can be noticed that the grain size is significantly larger compared to the material close to the weld root.*

Atomic Force Microscopy was applied to measure the depth and with of the grain boundary attack caused by the sodium citrate solution. After exposure for 24 hours, the grain boundaries where attacked to a depth of 0.8 nm and a width of 1.1 µm. An example is given in Figure 3-35. A similar rate of grain boundary corrosion was observed on the electron beam welded samples with the difference that the samples where only exposed for 2 hours, indicating that the friction stirred weld samples have a better corrosion resistance compared to the electron beam welded samples. This observation is in good agreement with the Scanning Kelvin Probe measurements of the surface potentials on the samples. In case of the electron beam welded samples a potential difference between weld and base material of ca 200 mV was obtained (Figure 3-5), while on the friction stirred weld sample the potential difference was ca 90 mV (Figure 3-9).

In summary, it was possible to induce grain boundary corrosion on copper canister materials (weld, heat affected zone and base materials) using a sodium citrate solution. However, the conditions induced by the solution (pH 4, 1 M NaCl) are long from the conditions present in the repository. Furthermore, the main attack of corrosion was observed on the welds in a “flow” type pattern that does not coincide with the grain structure of the electron beam welded samples. This type of corrosion might be due to residual stresses in the welds. It seems likely that the more general corrosion on the weld material protects the grain boundaries of the large copper crystals, since grain boundary attack was more predominant on the grains in the heat affected zone and even the base material compared to the weld area.

It could be noted that the friction stir welded samples have a much smaller grain size compared to the electron bream welded sampled. The former samples exhibit also a better corrosion resistance against the sodium citrate solution.

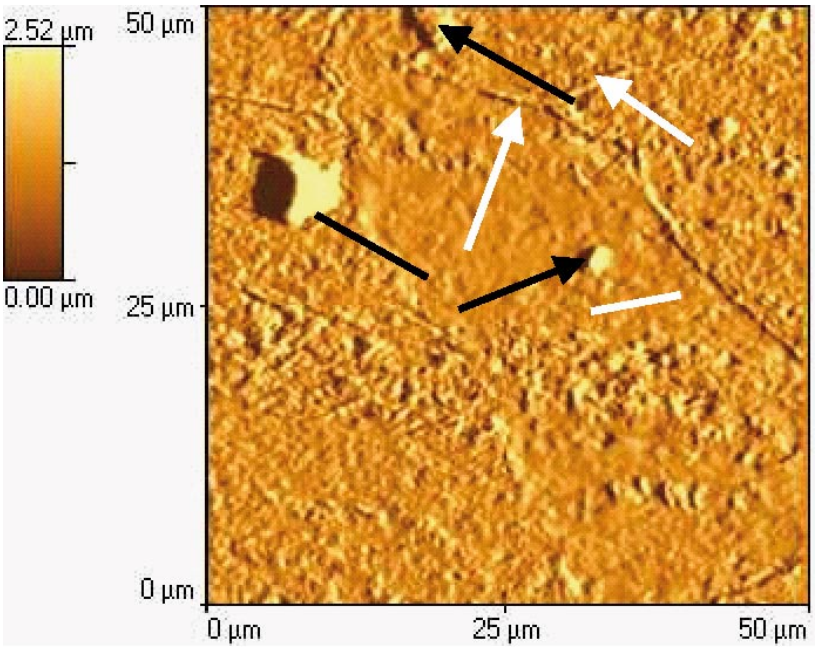

Figure 3-34. *Atomic Force Micrograph taken close to the weld root. Grain boundary corrosion (white arrows) and local corrosion (black arrows) was induced by the citrate solution.*

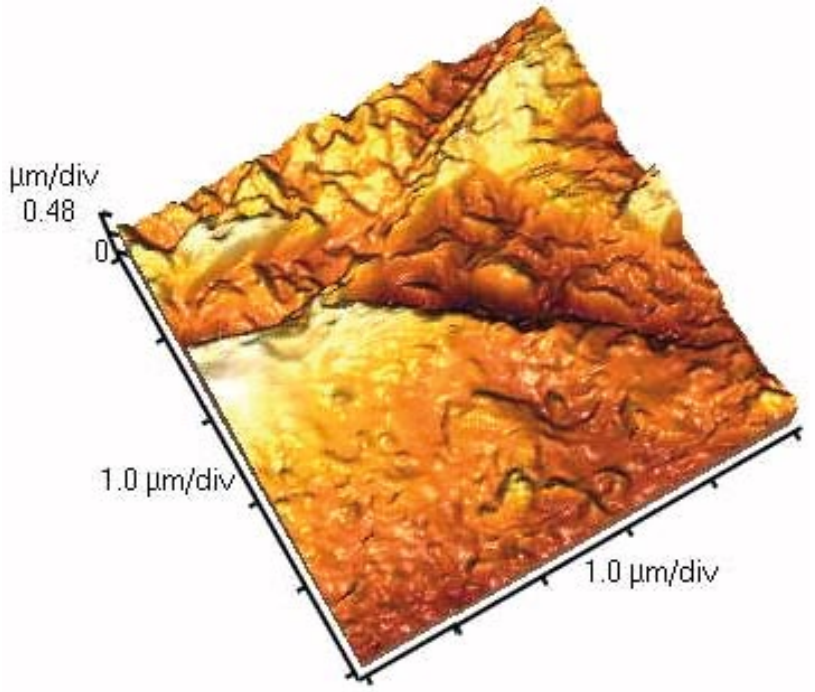

Figure 3-35. *3 dimensional Atomic Force Micrograph taken at the junction of three grains.*

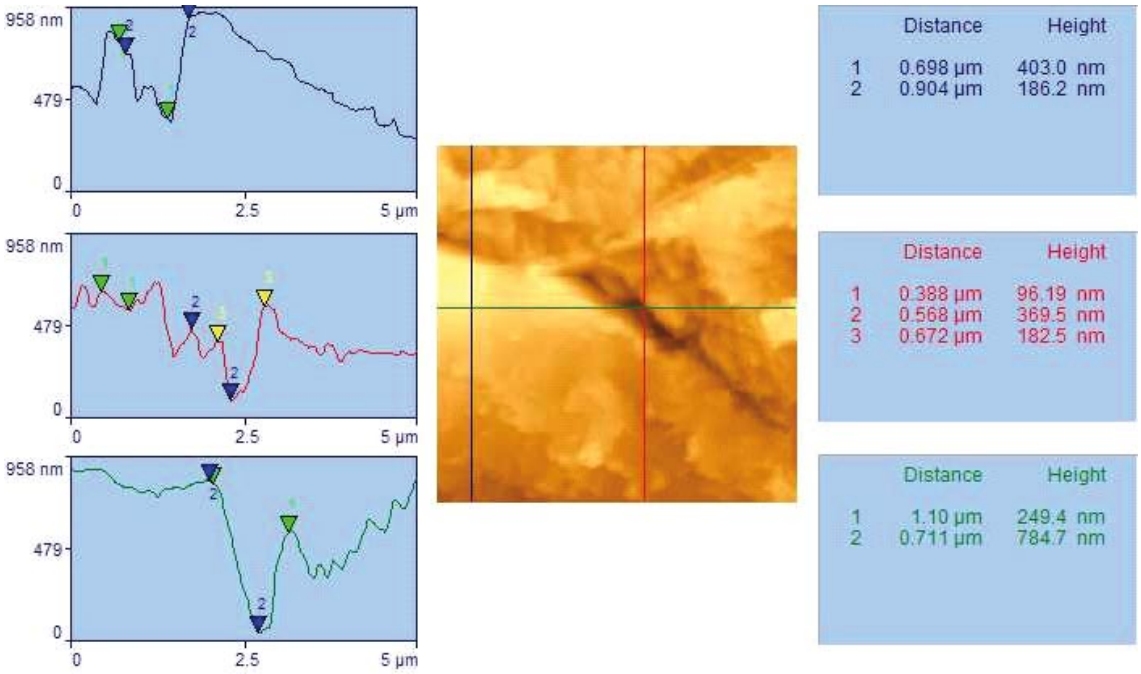

Figure 3-36. *Line analysis of the image shown in Figure 3-35. The grain boundaries have been corroded to a depth between 100 to 500 nm and a with between 0.4 to 1.1 µm.*

4 Conclusions

This investigation demonstrated that, although grain boundary corrosion could be induced on canister weld material, it is most unlikely a concern in the repository environment. The "stirring type" corrosion attack on the electron beam welds was much more predominant in the experiments performed than the very slight grain boundary corrosion observed. Although the friction stir welded samples also exhibited grain boundary corrosion, it was observed that the rate of corrosion was much smaller compared to the electron beam welded samples.

The relatively high surface potential differences (90–200 mV) between the weld material and base material could set up a corrosion cell with the weld material being a small anode and the base material a large cathode, leading to a higher corrosion rate of the welds compared to the rest of the canister.

5 Recommendations

No further investigations into grain boundary corrosion of canister material are seen to be necessary, since other corrosion attack resulted in much higher material loss than the observed attack on the grain boundaries.

Both types of welding methods have been improved and it would be interesting to investigate the galvanic effect of the welding procedures on current weld samples in artificial ground water using electrochemical techniques to verify that the prediction models for the long term corrosion resistance of the canisters are correct.

6 References

/1/ Grain Boundary Corrosion of Copper Canister Material. Fennel, P. A. H., Graham, A. J. Smart, N. R. and Sofield, C. J. SKB Technical Report TR-01-09.

/2/ The Corrosion of Copper, Tin and their Alloys, Leidheiser, H, Jr., Wiley, 1971.

/3/ Effect of surface orientation on the behaviour of intergranular corrosion of '<110>tilt epsilon 9' grain boundaries of high purity copper. Miyamoto, H, Yahashi, J., Yamashita, M., Mimaki, T. Science and Engineering Reviews of the Doshisha University; Vol 40; No 3, pp 1–9 October 1999 ABSTRACT.

/4/ Measurement of grain boundary corrosion on Copper[111]-tilt bicrystals by scanning vibrating electrode technique. Yamashita, M., Miyamoto, H, Yahashi, J., Uchida, H., Hashimoto, S., Mimaki, T., Materials Science Forum Vol. 294–296, pp 739–742, 1999 ABSTRACT.

/5/ Factors Influencing the Susceptibility to Intergranular Attack, Stress Corrosion Cracking and the de-alloying Attack of Aluminum Brass. Mazza F., Torchio S., Corrosion Science, Vol. 23, No 10, pp 1,053–1,072, 1983.

/6/ Comments on "SKB RG&D-Programme 98" Focused on Canister Integrity and Corrosion. Boyer William H, SKI Report 99:20.

/7/ On the atmospheric Corrosion of Metals which are Covered with thin Electrolyte Layers – I. Verification of the Experimental Technique. M. Stratmann and H. Streckel, (1990). Corros. Sci., 30, 681.

/8/ On the atmospheric Corrosion of Metals which are covered with thin Electrolyte Layers – II. Experimental Results. M. Stratmann and H. Streckel, (1990). Corros. Sci., 30, 697.

/9/ On the atmospheric Corrosion of Metals which are covered with thin Electrolyte Layers – III. The Measurement on Metal Surfaces which are covered by thin Electrolyte Layers. M. Stratmann, H. Streckel, K.T.Kim and S.Crockett, (1990). Corros. Sci., 30, 715.

ISSN 1404-0344
CM Digitaltryck AB, Bromma, 2005